Sedimentary Geology 405 (2020) 105705

Contents lists available at ScienceDirect

Sedimentary Geology

journal homepage: www.elsevier.com/locate/sedgeo

Eocene carbonate accumulation in the north-central Pacific Ocean: new insights from Ocean Drilling Program Site 1209, Shatsky Rise

Joyeeta Bhattacharya *, Gerald R. Dickens

Department of Earth, Environmental and Planetary Sciences, Rice University, Houston, TX 77005, USA

ARTICLE INFO

Article history:
Received 2 April 2020
Received in revised form 29 May 2020
Accepted 1 June 2020
Available online 6 June 2020

Editor: Dr. Brian Jones

Keywords:
Eocene climate
Carbonate dissolution
Hyperthermals
Lysocline
Carbon cycle

ABSTRACT

Major climate transitions and perturbations in global carbon cycle are known to have occurred during the Eocene, between 56 and 34 million years ago (Ma). A series of carbon isotope excursions (CIEs) mark variations in the global carbon cycle and changes in climate through early Eocene. Paleocene-Eocene Thermal Maximum (PETM) ca. 56 Ma is the most pronounced and well documented of these events expressed as a clay rich layer in many deep-sea sections, resulting from widespread carbonate dissolution on the seafloor, which is in turn related to shoaling of the carbonate compensation depth (CCD) and lysocline. Other CIEs of early Eocene had similar response. However, response of these geologically 'instantaneous' hyperthermals differ from long-term warmth (multi-million-year time scale) of the Early Eocene Climate Optimum (EECO) in terms of sea-floor carbonate accumulation. Following the termination of EECO, earth's climate transitioned into long-term cooling. Pronounced fluctuations in CCD of equatorial Pacific are known to have occurred during middle-late Eocene as well, whose global extent and origin are still unresolved. Most proxy records either span the interval of early Eocene or document particular climatic events in Eocene, which significantly limits visualizing the long-term Eocene climate change and response of open marine carbonate preservation. The present study documents change in carbonate dissolution and carbonate mass accumulation rate through the entire Eocene (56–34 Ma) at ODP Site 1209 on Shatsky Rise, north-central Pacific and ties it to a stable carbon and oxygen isotope record. Our study determines the correlation between deep-sea carbonate dissolution and carbon cycling process during the dynamic climate regime of Eocene. A strong correlation between magnitude of CIEs and intensity of dissolution for early Eocene hyperthermal events appears to significantly weaken for multiple dissolution events in middle-late Eocene, thereby indicating fundamental difference in their causal mechanism.

© 2020 Elsevier B.V. All rights reserved.

1. Introduction

The Eocene, between approximately 56 and 34 million years ago (Ma), encapsulates major transitions and perturbations in Cenozoic climate (Fig. 1; Zachos et al., 2001, 2008; Cramer et al., 2009). On the broad, multi-million-year scale, Earth's surface warmed from the middle Paleocene to the Early Eocene Climate Optimum (EECO) circa 53 to 49 Ma (Luciani et al., 2016; Westerhold et al., 2018), when average surface and deep water temperatures likely exceeded those of present-day by at least 10 °C (Pagani et al., 2005; Hollis et al., 2009; Cramwinckel et al., 2018). Following EECO, significant cooling transpired through the latest Eocene (Zachos et al., 2001; Bijl et al., 2009; Bijl et al., 2013). Superimposed on these long-term changes, a number of geologically rapid warming events occurred (Zachos et al., 2004; Agnini et al., 2009; Lauretano et al., 2016). These "hyperthermals" include the well-known Paleocene-Eocene Thermal Maximum (PETM) at ~56 Ma (Westerhold et al., 2009, 2018; Kirtland Turner, 2018), the H-1/ETM-2, K/X/ETM-3 and at least four more events between 54 and 51 Ma (Lauretano et al., 2015; Westerhold et al., 2018). Additionally, a major global warming event the Middle Eocene Climate Optimum (MECO) occurred at ~40.5 Ma (Bohaty and Zachos, 2003; Boscolo Galazzo et al., 2014; van der Ploeg et al., 2018; Cramwinckel et al., 2019).

Although long-term and short-term variations in Eocene climate likely have different causes, they are widely thought to be linked to past changes in atmospheric pCO_2. Support for this idea comes from various proxies for pCO_2 (Beerling and Royer, 2011; Pagani et al., 2011; Hönisch et al., 2012; Anagnostou et al., 2016), but temporal and quantified relationships remain uncertain. More indirectly, stable carbon and oxygen isotope ($\delta^{13}C$, $\delta^{18}O$) records of benthic foraminifers across some intervals of the Eocene (Fig. 1; Zachos et al., 2001, 2008; Cramer et al., 2009) exhibit similar trends and patterns. In particular, from the middle Paleocene through part of the EECO, relatively lower/higher $\delta^{18}O$ values, which presumably indicate warm/cold conditions, align with lower/higher $\delta^{13}C$ values (Fig. 1), which presumably relate to greater/lesser inputs of organic carbon to the ocean and atmosphere (Dickens, 1995; Cramer et al., 2009; Stap et al., 2010). There are also records of carbonate accumulation in deep-sea sediment sections. During

* Corresponding author.
E-mail address: jb79@rice.edu (J. Bhattacharya).

https://doi.org/10.1016/j.sedgeo.2020.105705
0037-0738/© 2020 Elsevier B.V. All rights reserved.

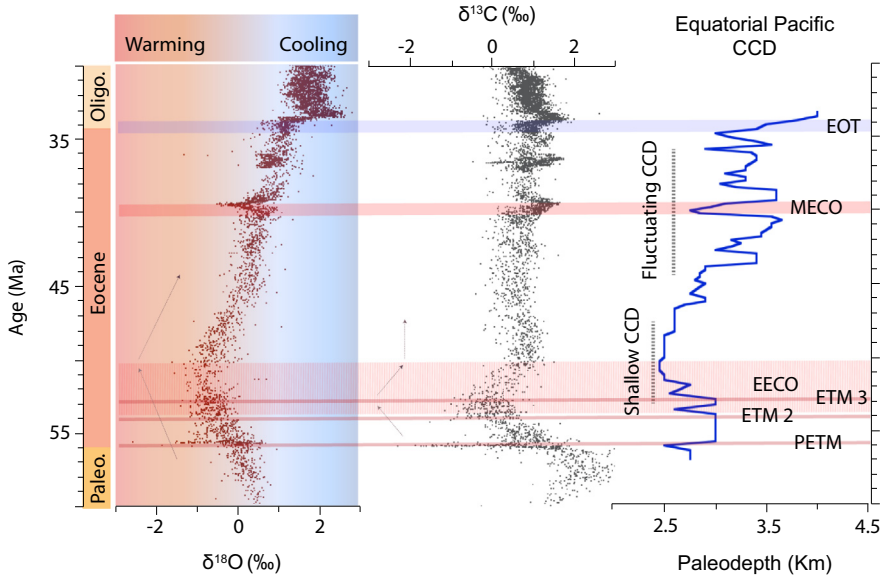

Fig. 1. Global composite Eocene isotope record and equatorial Pacific CCD reconstruction. The global composite carbon and oxygen isotope record from benthic foraminifers (Cramer et al., 2009) depicts changes in climate and carbon cycling during the Eocene epoch which is bounded by major perturbations in global carbon cycle. It begins with the warmest interval of the Cenozoic, i.e. Paleocene-Eocene Thermal Maximum (PETM), ca. 56 Ma and ends with the onset of icehouse conditions and first polar glaciation of the Cenozoic at Eocene-Oligocene transition (EOT), ca. 34 Ma. The dashed lines with arrowheads show the overall change in trend of $\delta^{13}C$ and $\delta^{18}O$ during early Eocene. The equatorial Pacific CCD (Pälike et al., 2012) shoaled during PETM and parts of EECO, and exhibits major fluctuations through middle-late Eocene. Post early Eocene, it was deepening on long time scale.

the prolonged period of greenhouse warmth heading into EECO, when carbon inputs into the combined ocean-atmosphere system were presumably higher and coupled with enhanced weathering (Kump et al., 2000; Penman et al., 2016; Greene et al., 2019), carbonate saturation horizons in the deep ocean should have deepened (Hancock et al., 2007; Kump et al., 2009; Slotnick et al., 2015). By contrast, during early Eocene hyperthermals, and presumed rapid and massive carbon injection, shoaling of carbonate saturation horizons should have occurred (Dickens et al., 1997; Zachos et al., 2005). Notably, these predicted divergent responses (Fig. 2; Berner et al., 1983; Ridgwell and Zeebe, 2005; Kirtland Turner and Ridgwell, 2016) have been previously documented (Hancock et al., 2007; Leon-Rodriguez and Dickens, 2010; Slotnick et al., 2015; Penman et al., 2016).

Intuitive links between global climate and carbon cycling begin to "break-down" in the middle of EECO (Fig. 1). With available records (Zachos et al., 2008; Luciani et al., 2016; Westerhold et al., 2017, 2018), there is a nominal 1‰ rise in the $\delta^{13}C$ of marine carbonate at about 50 Ma, and values remain relatively constant through the remainder of the Eocene. Furthermore, records from the equatorial Pacific suggest generally increasing deep-sea carbonate accumulation from the middle to late Eocene, albeit with major variations (Lyle et al., 2005; Pälike et al., 2012). To link changes in early Eocene climate and deep-sea carbonate accumulation, most studies have focused on sites close to carbonate compensation depth (CCD). While such an approach is appropriate for paleo-CCD reconstructions (Leon-Rodriguez and Dickens, 2010; Pälike et al., 2012; Slotnick et al., 2015), it limits full assessment of deep-sea carbonate accumulation, because considerable changes might occur above the CCD and because sites near the CCD do not record carbonate during intense ocean acidification. In this regard, it seems important to study sites that lie well above CCD and hence accumulate carbonates for long periods of time.

Ocean Drilling Program (ODP) Site 1209 in the north-central Pacific was well above the CCD throughout the Paleogene (Fig. 2; Bralower et al., 2002) and hence presents an excellent opportunity to study changes in open marine carbonate accumulation across the Eocene. Here we examine sediments at Site 1209, including detailed measurements of proxies for carbonate dissolution, such as planktic foraminiferal fragmentation and planktic to benthic foraminiferal ratios (Hancock and Dickens, 2005; Colosimo et al., 2006; D'Onofrio et al., 2020). These dissolution proxy records are then combined with carbonate accumulation rates, $\delta^{13}C$ and $\delta^{18}O$ records at Site 1209 to constrain links between deep-sea carbonate preservation, carbon cycling and climate change across the Eocene. Upfront, it should be noted that one conclusion is that vertical movements of the sea floor, especially in the Pacific and during the late-early Eocene (e.g. Sutherland et al., 2020) may impact interpretations.

2. Background

2.1. Present day deep ocean carbonate accumulation

Within the modern pelagic realm, sediments with significant calcium carbonate (>10%) cover approximately 50% of the seafloor (Archer, 1996). The $CaCO_3$, principally calcite, derives from postmortem rain of tests precipitated in the photic zone by coccolithophores and planktic foraminifers. Carbonate ion concentrations [CO_3^{2}] generally decrease with water depth, because of respiration of organic carbon, higher dissolved [CO_2] and lower pH (Broecker and Peng, 1982). Carbonate saturation in ocean water depends on concentrations of Ca^{2+} and CO_3^{2-} ions in ambient waters and the solubility constant (K_{sp}) of $CaCO_3$:

$$\Omega = \left[Ca^{2+}\right]\left[CO_3{}^{2-}\right]/K_{sp} \quad (1)$$

where K_{sp} depends on pressure and temperature (Mucci, 1983; Millero, 1995; Ridgwell and Zeebe, 2005). Consequentially, a predicted water column depth exists where carbonate should precipitate above and dissolve below.

Transfer of calcite solubility conditions to the sedimentary record becomes complicated because of kinetics, mineralogy and burial (Ridgwell and Zeebe, 2005). In general, for open marine conditions (aka without terrigenous dilution), and from the perspective of the sedimentary record, there are two main horizons related to marine carbonate saturation (Fig. 2): a relatively deep carbonate compensation depth (CCD), below which almost no

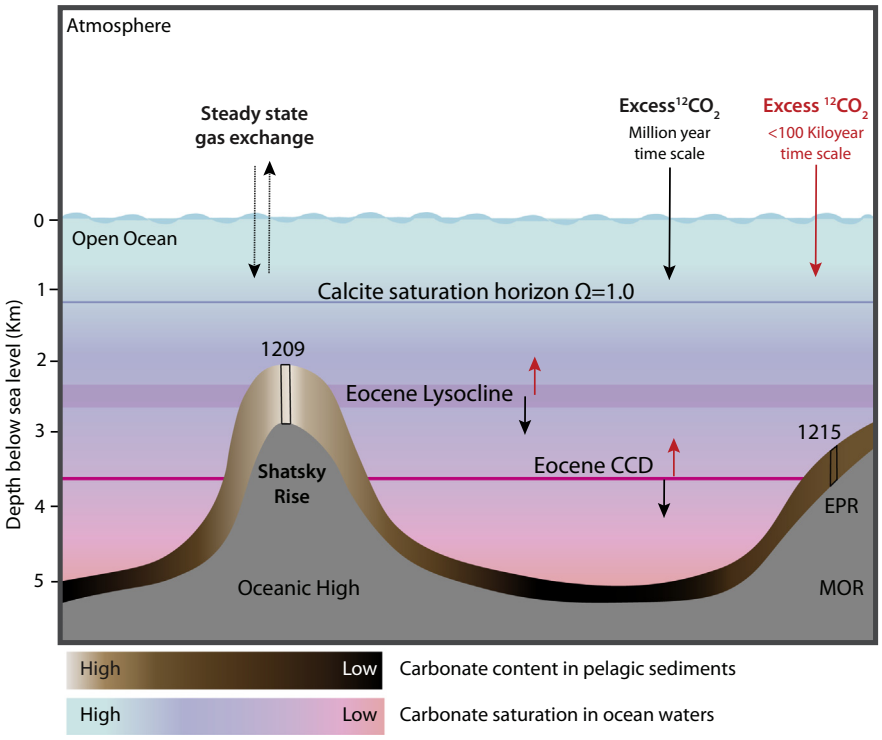

Fig. 2. Realms of carbonate dissolution. Carbonate Compensation Depth (CCD) and lysocline respond to changes in ocean's dissolved CO_2 which is in turn controlled by global carbon cycling and timescale of CO_2 input into ocean-atmosphere system. Input of excess ^{12}C depleted CO_2 in long-term (million year) time scale into the system will be gradually responded by negative feedback mechanism (e.g. silicate weathering) and result in deepening of saturation horizons by increased carbonate burial. In contrast to this process, a rapid ^{12}C depleted CO_2 input (<100 kiloyear time scale) will not be able to start the negative feedback processes, and rather result in compensation by shoaling of saturation horizons, i.e. CCD and lysocline and cause increased deep-sea carbonate dissolution across a short interval of time. Hence CCD and lysocline remain dynamic through time, as carbon cycle processes operate differently in response to different rates of CO_2 input in the ocean-atmosphere system. EPR in this figure is East Pacific Rise and MOR denotes Mid Oceanic Ridge.

carbonate accumulates, and an overlying lysocline, where carbonate saturation starts declining sharply and carbonate content decreases below 80% (Zeebe and Westbroek, 2003; Ridgwell and Zeebe, 2005; Boudreau et al., 2010). These vary in depth throughout the modern ocean, because of differences in temperature, deep water chemistry, the supply of carbonate from the photic zone, and processes at or near the seafloor (Archer, 1996). In general, at present-day, the CCD and lysocline are deeper in the Atlantic than in the Pacific, and deeper in tropical regions than at higher latitudes (Ridgwell and Zeebe, 2005). Of interest to this study, within the present-day tropical north-central Pacific, the CCD lies between 4200 and 4800 mbsl on average (Broecker, 2008; Sulpis et al., 2018), and the lysocline extends ~1000 m above this (Archer, 1996).

Variability in carbonate accumulation also arises from differences in mineralogy and morphology of carbonate tests. Of particular relevance to the pelagic realm, compact coccoliths, while typically <20 μm across, consist of near pure calcite (Cros and Fortuño, 2002) with low surface area/volume ratios. By contrast, hollow planktic foraminiferal tests, while typically >63 μm across, consist of calcite with significant amounts of Mg and high surface area/volume ratios, especially when they have abundant pores in the test wall (Boudagher-Fadel, 2018). In general, a pattern of dissolution emerges amongst calcite tests: calcareous nannoplankton are most resistant, benthic foraminifers are moderately resistant, planktic foraminifers are least resistant (Thunell, 1976; Berger et al., 1982; Nguyen et al., 2009). Amongst planktic foraminifers, though, dissolution resistance varies widely across different genera (Petrizzo et al., 2008; Nguyen et al., 2009). Differential dissolution leads to preferential fragmentation of planktic foraminifers in seafloor sediments, especially below the lysocline (Berger, 1973; Shackleton and Hall, 1984; Reghellin et al., 2015).

2.2. Deep-ocean carbonate accumulation during the Paleogene: concepts and reconstructions

Sea floor carbonate accumulation is well established for modern day ocean basins (Berger et al., 1976; Broecker and Peng, 1982; Archer, 1996; Ridgwell and Zeebe, 2005). However, this has changed over time because of variations in carbon inputs to the ocean and atmosphere, the dominant locus of marine carbonate burial (shelf-basin fractionation), and the net path of deep-water flow. Here it is good to consider that the modern exogenic carbon cycle consists of the ocean, atmosphere and biosphere with a total mass of nominally 40,000 Pg C, total carbon inputs and outputs of nominally 0.4 Pg C/yr, a residence time of nominally 100 kyr, and an internal carbon cycling time of nominally 1000 yr (Berner, 1991; Kump, 1991; Dickens, 2003; Sluijs et al., 2013).

From a long-term viewpoint (>200 kyr), the total amount of carbonate buried in the pelagic realm should equal inputs to the exogenic carbon cycle after accounting for carbonate buried in shallow marine environments and organic carbon buried in both environments (Ridgwell and Zeebe, 2005; Pälike et al., 2012; van der Ploeg et al., 2018). This necessarily implies some basic expectations (Fig. 2). During long times of elevated carbon delivery (e.g., through enhanced volcanism), carbonate accumulation in the overall ocean should increase; during times of reduced carbonate accumulation along continental margins, carbonate accumulation in the deep ocean should increase. In both cases, the CCD and lysocline should deepen. Alternatively, from a short-term viewpoint (<50 kyr or half the residence time), one needs to consider distributions of dissolved carbon species and advection through the ocean. In particular, a rapid injection of CO_2 to the ocean or atmosphere should shift [CO_3^{2-}] to bicarbonate [HCO_3^-], which should temporarily shoal the CCD and lysocline (Fig. 2).

Pioneering work by van Andel (1975) readily demonstrated major changes in the CCD of the Pacific and Indian oceans over the Cenozoic.

This work was accomplished by placing carbonate content data down sediment sequences from multiple Deep-sea Drilling Project (DSDP) sites into a time-water depth perspective. A basic finding was a relatively shallow Indo-Pacific CCD during the Eocene (~3400 m depth) and a major deepening near the Eocene-Oligocene Boundary. Subsequent work, using more recently collected DSDP/ODP/IODP sequences or re-investigating original sequences in greater detail confirm these basics, but also highlight the dynamic nature of the CCD during the Eocene (Rea and Lyle, 2005; Pälike et al., 2012; Slotnick et al., 2015), an aspect that could not be recognized initially, mostly due to low temporal resolution of carbonate content data.

Since 1975, a vastly improved understanding of carbon cycling and climate during the early Eocene has emerged (Kump and Arthur, 1999). Much of this has come through detailed stable isotope records of carbon and oxygen ($\delta^{13}C$, $\delta^{18}O$) measured in various phases, which correlate across numerous sites (e.g. Keith and Weber, 1964; Shackleton et al., 1985; Zachos et al., 2001, 2008; Cramer et al., 2009). A key finding is that major changes in carbon cycling and climate transpired during the early Eocene. As an outstanding example, major negative excursions in $\delta^{13}C$ and $\delta^{18}O$ happened across the PETM and several other younger events, and these have been linked to massive input of CO_2 to the exogenic carbon cycle (Dickens, 1995; Dickens et al., 1997; Zachos et al., 2007, 2010). Consistent with theory (Dickens et al., 1997), analyses of sediment records show that rises in the CCD and lysocline also occurred during this event (Lu and Keller, 1993; Thomas and Shackleton, 1996; Hancock and Dickens, 2005; Colosimo et al., 2006). There is now considerable interest in more fully coupling stable isotope records with those for carbonate accumulation across the Eocene (Zachos et al., 2001; Leon-Rodriguez and Dickens, 2010; Slotnick et al., 2015; Greene et al., 2019).

Previous work regarding carbonate accumulation in the Eocene deep ocean mostly has focused on CCD reconstructions (e.g., van Andel, 1975; Leon-Rodriguez and Dickens, 2010; Pälike et al., 2012; Slotnick et al., 2015). However, to expand on commentary above, this approach limits perspectives for two reasons. First, numerous scientific drill sites have Eocene sediments that accumulated at intermediate water depths (1500–3000 m) and consistently above the CCD (Bralower et al., 2002; Zachos et al., 2004). Second, the CCD at a given location and time gives little information on the distribution of carbonate accumulation at shallower water depths (Greene et al., 2019). Significant carbonate dissolution happens below lysocline and dissolution progressively increases towards CCD (Ridgwell and Zeebe, 2005; Boudreau et al., 2010). Therefore, a complimentary approach towards understanding pelagic carbonate accumulation and carbon cycling during the Eocene is to decipher past changes in the lysocline, specifically by generating records of carbonate accumulation and $\delta^{13}C$ at sites located at intermediate water depths. Such an effort initiated with preliminary work at drill sites on Shatsky Rise (e.g. Hancock and Dickens, 2005; Colosimo et al., 2006).

3. Material and methods

3.1. Site 1209

Shatsky Rise, a large igneous province located in the northwest Pacific (Fig. 3), rises from surrounding abyssal plains to water depths of ~2000 m (Sager et al., 1999). It consists of three prominent highs, the largest being Southern High (Bralower et al., 2002). Shatsky Rise probably originated in the Equatorial Pacific during the Late Jurassic and moved north and then northwest to its current location (Sager et al., 1999; Bralower et al., 2002). Far from continental margins, it serves as an excellent location to collect and study open ocean Paleogene sediment sequences (Bralower et al., 2002).

Samples for the present work come from Site 1209 of ODP Leg 198. The site lies at 32°39.10′N, 158°30.36′E and 2387 m water depth, near the highest elevation of Southern High (Bralower et al., 2002; Dutton et al., 2005). Three holes (A, B and C) were drilled, which extend to ~320 m below sea floor (mbsf). This includes ~297 m of sediments described as nannofossil ooze and nannofossil ooze with clay (Bralower et al., 2002). Minor biogenic components include foraminifers, diatoms, radiolarians and fish teeth, while minor non-biogenic components include pyrite, iron oxides and zeolites (Bralower et al., 2002).

Significant changes in color and physical properties characterize sediments at Site 1209 (Fig. 4). By aligning such variations, particularly magnetic susceptibility (MS), sediment cores from the three holes can be spliced together to construct a composite section with a common depth frame (Bralower et al., 2002). For this study, we use a revised meters composite depth (rmcd) scale (Westerhold and Röhl, 2006). The composite section at Site 1209 holds an almost continuous record of early Paleogene sediment with high (generally >80 wt%) carbonate content. Although the site migrated northward during the early Paleogene, it remained <2500 m below sea level (Bralower et al., 2002; Dutton et al., 2005) and above the CCD (Colosimo et al., 2006; Rea and Lyle, 2005). Given present and past water depths, the site should record variations in the regional lysocline, particularly those that potentially occurred during Eocene long- and short-term changes in climate and

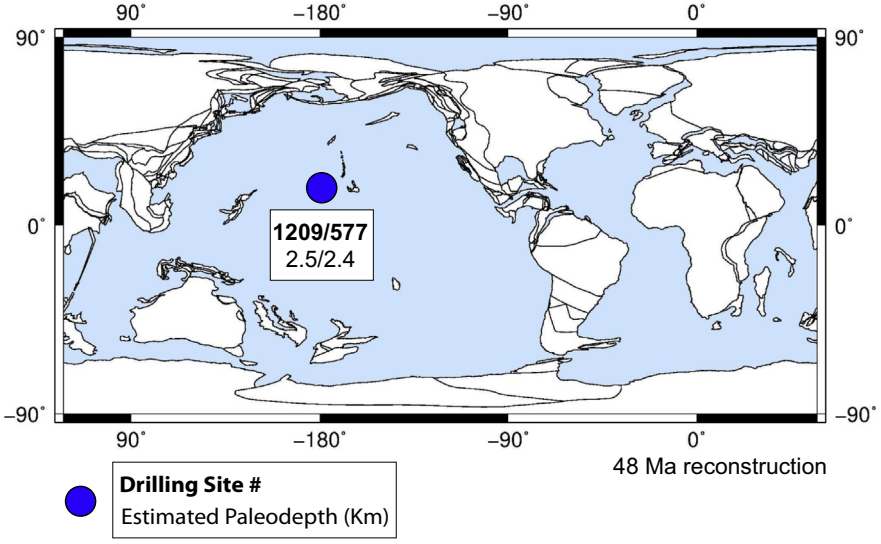

Fig. 3. Location of Shatsky Rise. 48 Ma map showing reconstructed tectonic plates and Sites 1209 and 577 on Shatsky Rise. (www.odsn.de).

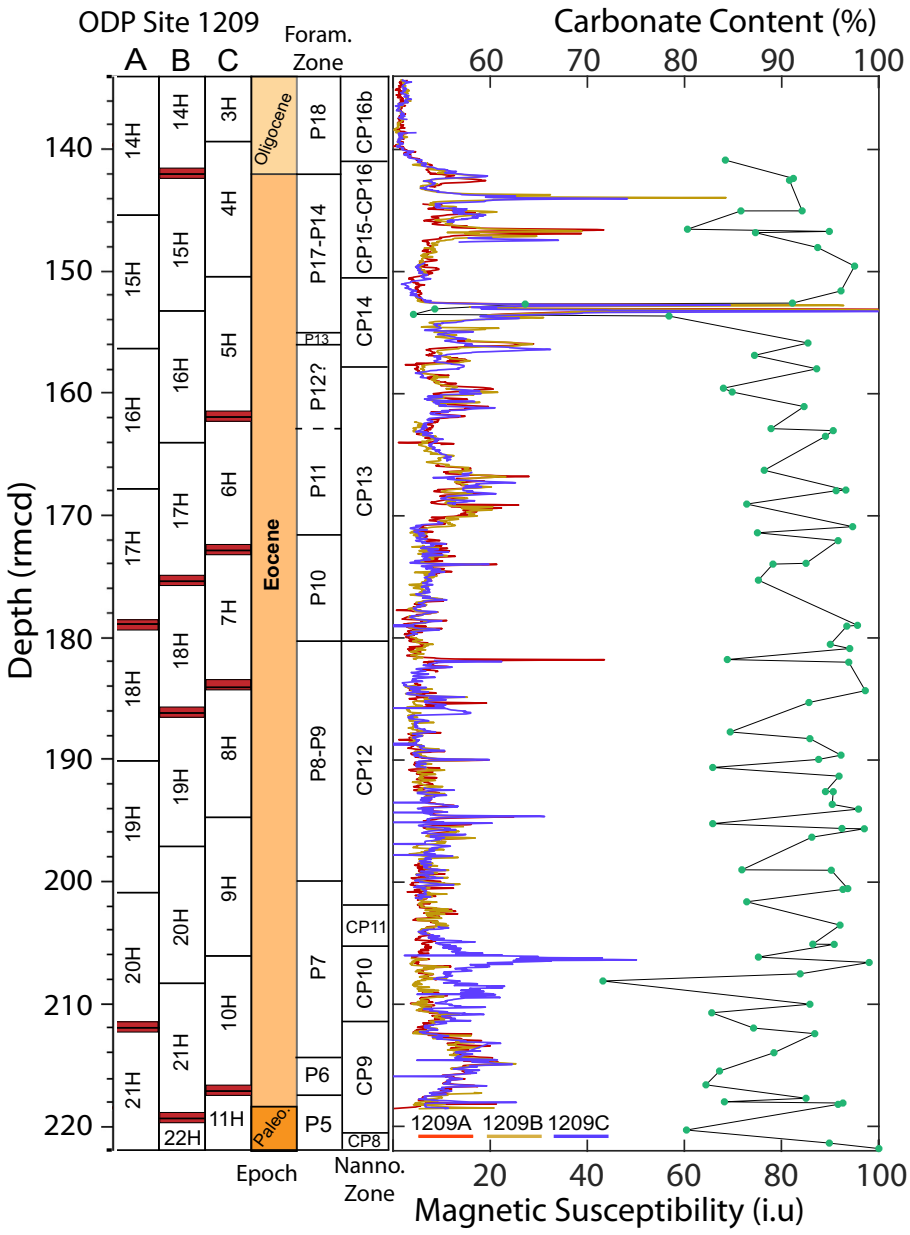

Fig. 4. General description of Eocene sediments from Site 1209. Biostratigraphic zones of Site 1209 are adapted from Bralower et al., 2002 (where calcareous nannofossil biozonation follows Okada and Bukry, 1980 and planktic foraminiferal zonation follows Berggren et al., 1995). Alongside are shown downhole variations of magnetic susceptibility (Bralower et al., 2002) and carbonate content (Hancock and Dickens, 2005; Bralower et al., 2002).

carbon cycling (Bralower et al., 2002; Colosimo et al., 2006; Stap et al., 2009).

Previous studies on early Paleogene deep ocean sediments have used weight percent coarse fraction as one proxy for carbonate dissolution (Hancock and Dickens, 2005; Kelly et al., 2010; Luciani et al., 2016). This relies on the argument that planktic foraminifers dominate the coarse fraction, and they dissolve easier than fine-grained calcareous nannoplankton (Berger et al., 1982; Chiu and Broecker, 2008; Hancock and Dickens, 2005; Kelly et al., 2010; Luciani et al., 2016; Reghellin et al., 2020). Hence, during a given interval of ocean acidification (e.g., an early Eocene hyperthermal), the coarse fraction weight percent should decline. However, results from earlier studies at Site 1209 show a significant increase in coarse fraction across the PETM (e.g. Hancock and Dickens, 2005; Westerhold et al., 2018). Clearly, interpretations of this proxy for carbonate dissolution are complicated, and while beyond the scope of this study, may be worthy of future research.

3.2. Samples and sedimentation rates

We collected 333 samples between 134.32 and 220.14 rmcd (Supplementary Table 1). The depth interval belongs to lithostratigraphic Subunit IIA, accumulated from the latest Paleocene to earliest Oligocene, and consists of mostly carbonate (typically >80 wt%). The subordinate non-carbonate portion of sediments comprises clay, fish teeth and biosilica (Bralower et al., 2002). Total sample numbers include 278 from Hole A, 33 from Hole B, and 22 from Hole C. Samples were collected using 10 cc plastic scoops at Gulf Coast Repository, College Station, TX.

Sedimentation rate (SR) functions can be estimated using calcareous nannofossil biostratigraphy (Bralower, 2005). First and last occurrence datum intervals from Bralower (2005) have been assigned ages in accordance with GTS 2012, based on Agnini et al. (2016) and Norris et al. (2014). We offer two "end-member" possibilities: a stepped linear

function and a smoothed function (Fig. 5). SR dropped from ~6 to 2 m/my between 57 and 53 Ma, reached a high to 9 m/my between 49 and 44 Ma, and remained between ~4 and 2 m/My between 44 and 35 Ma.

All 333 samples were oven-dried at 60 °C for 24 h to remove remaining pore water. Each dried sample was split into two aliquots. One aliquot was crushed and homogenized using an agate mortar and used for carbonate content and stable isotope analyses. The other half was used for foraminiferal "dissolution" studies.

3.3. Analytical methods

3.3.1. Stable isotopes

Bulk sediment stable isotope compositions were determined using ~100 μg of powdered and homogenized material. Samples from Hole A were analyzed on an Isotope Ratio Mass Spectrometer (IRMS) coupled to a Kiel IV carbonate device at the Stable Isotope Laboratory, University of California, Santa Cruz. Carbon and oxygen isotope measurements were calibrated to Vienna PeeDee Belemnite (vPDB) using NBS-18, CM-12 and in-house standard Atlantis II. Samples from Holes B and C were analyzed on an IRMS coupled with a Gasbench II device at the Stable Isotope Laboratory, Rice University. Weights of samples used for these analyses were adjusted to obtain approximately 150 μg of carbonate. Measurements were calibrated to Vienna PeeDee Belemnite (vPDB) using NBS-18, IAEA-603 and in-house KLS as standards. Analytical precision was better than ±0.05‰ for $\delta^{13}C$ and ± 0.1‰ for $\delta^{18}O$ (UCSC), and ± 0.1‰ for $\delta^{13}C$ and ± 0.2‰ for $\delta^{18}O$ (Rice U). True replicates of 26 samples were analyzed at both laboratories, yielding maximum differences of 0.15‰ for $\delta^{13}C$ and 0.3‰ for $\delta^{18}O$.

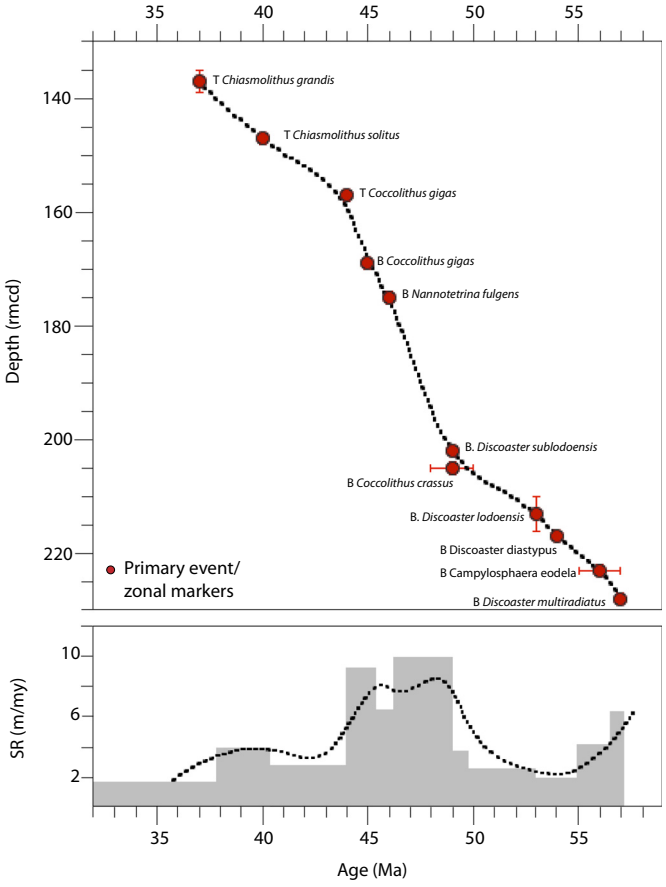

Fig. 5. Sedimentation rate at Site 1209. Primary event/zonal markers from calcareous nannofossil biostratigraphy (Bralower, 2005) are displayed in the age-depth relationship curve. Top and bottom of such datum planes have been designated as T and B respectively. These markers have been used to calculate sedimentation rate (SR), shown on the bottom panel. The dotted line marks a smooth SR function.

3.3.2. Carbonate content and mass accumulation rate

Carbonate content was determined at Rice University using the 'Karbonat-bombe' technique (Dunn, 1980; Müller and Gastner, 1971). Approximately 2 g of sediment was weighed and subsequently reacted with 10 ml of 10% hydrochloric acid in a chamber connected to a water-filled burette. The 333 samples were analyzed in batches with variable masses (1.5 to 5 g) of reagent grade calcium carbonate and BCSS-CRM No. 393 Limestone as standards. Analytical precision was within ±2%, as determined from multiple measurements of standards.

The carbonate mass accumulation rate (MAR_{carb}, in g/cm^2/ky) for a given sample can be calculated by the following equation using the SR (van Andel, 1983; Norris et al., 2014):

$$MAR_{carb} = SR * (CaCO_3\ wt\%/100) * DBD, \quad (2)$$

where SR is sedimentation rate (cm/ky) and DBD is dry bulk density (g/cm^3) (Supplemental Fig. 1), which includes grain density and pore space.

3.3.3. Dissolution proxies

Dissolution of foraminiferal tests occurs during postmortem descent through the water column and on or near the seafloor. Two proxies for this process have been suggested: the degree of planktic foraminiferal fragmentation and the ratio of planktic to benthic foraminifers (Berger, 1970; Bé et al., 1975). These indices have been measured in several studies on deep-sea Paleogene sediment cores (Hancock and Dickens, 2005; Leon-Rodriguez and Dickens, 2010; Luciani et al., 2016; D'Onofrio et al., 2020). In this study, we follow previous work but place extra effort on documenting how such indices are determined.

Approximately 10 g of each dried sample was gently, cautiously and thoroughly mixed with deionized water and sieved at >63 μm. For deep-sea sediment well above the CCD, this leads to a coarse fraction typically comprised of foraminifers (Bassinot et al., 1994; Frenz et al., 2005; Chiu and Broecker, 2008). After drying overnight on filter paper, the coarse fractions were put into an oven for 24 h at a fixed temperature of 60°C, to remove excess moisture. Using a stereoscope, planktic foraminifers were counted for whole tests (w) and fragments (f) and benthic foraminifers were counted for moderate to well preserved tests (b). At least 300–500 counts were made per sample to minimize statistical bias (Malmgren, 1987). Twenty-five samples were sieved and processed separately and re-counted to ascertain reproducibility. In general, two types of foraminiferal test fragments occur. A "type 1" fragment (f1) is where the test portion is less than two thirds of its supposed original size (Berger et al., 1982; Hancock and Dickens, 2005). A "type 2" fragment (f2) is where a test exhibits significant signs of peeling on wall structure (Leon-Rodriguez and Dickens, 2010). Representative samples to demonstrate different types of foraminifers and fragments (w, b, f1 and f2) are shown in Fig. 6.

The fragmentation index (FRAG) was calculated for planktic foraminifers using the following formula (Le and Shackleton, 1992; Hancock and Dickens, 2005; Leon-Rodriguez and Dickens, 2010):

$$FRAG\ (\%) = \{(f/8)/[(f/8) + w]\}/100. \quad (3)$$

The "eight" in the equation is a somewhat arbitrary value to provide a more linear response of foraminiferal fragmentation; effectively, a single planktic foraminifer breaks into multiple fragments (Le and Shackleton, 1992). Also, by convention, benthic foraminifers were not counted as part of the number of whole foraminifers, because benthic foraminifers tend to be more resistant to dissolution (Berger, 1973; Nguyen et al., 2009).

The planktic/benthic index (P/(P + B)) is defined as the number of whole planktic foraminiferal tests (w, which is the same as used for calculating FRAG) divided by the sum of whole planktic foraminiferal

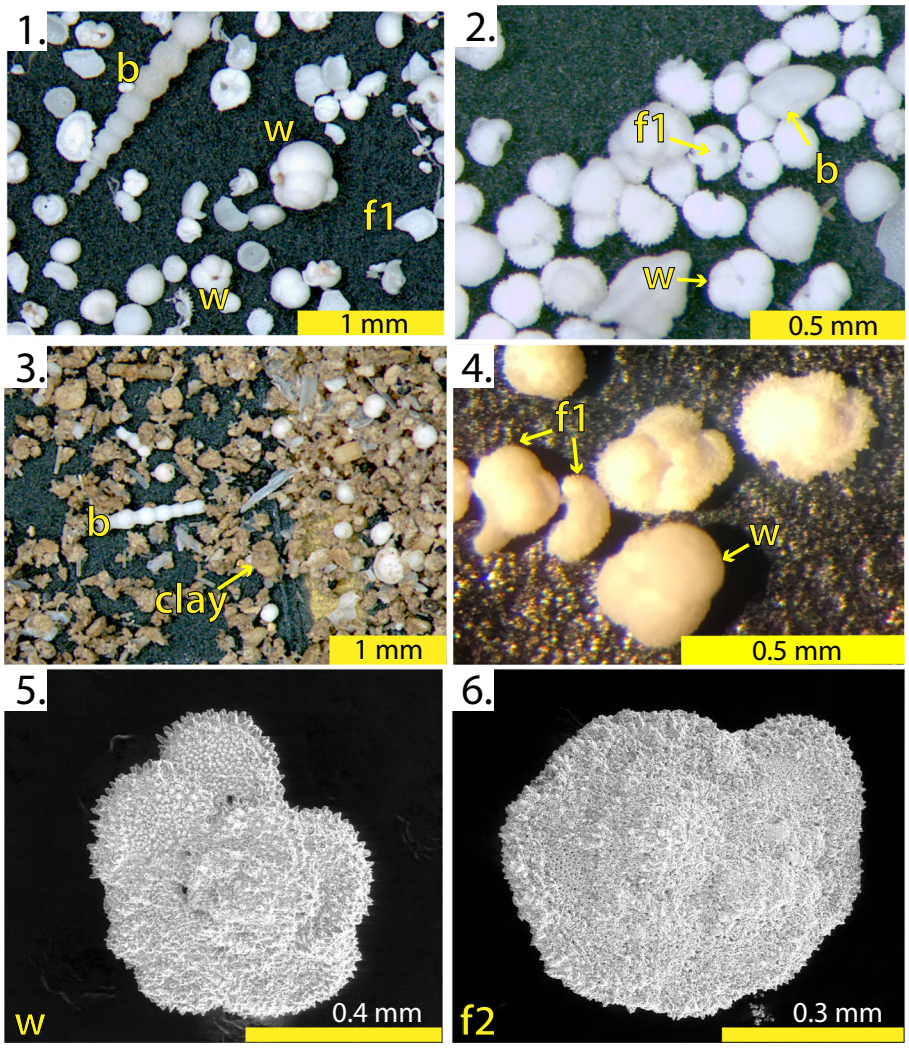

Fig. 6. Methods of calculating FRAG and P/P + B. 1–4. Stereomicroscopic imagery of different samples and foraminifers. 'w' denotes a whole/complete planktic foraminifer while, 'b' denotes a moderately-well preserved benthic foraminifer and 'f' denotes a fragment. 5–6. SEM imagery of planktic foraminifer (genus *Morozovella*). 5. shows a whole test (w), while 6. can be considered as a type 2 fragment (f2), showing significant dissolution of muricae.

(w) and moderately to well preserved benthic foraminiferal tests (b) (Leon-Rodriguez and Dickens, 2010). More specifically:

$$P/(P+B) = w/(w+b). \quad (4)$$

As both indices involve extensive and subjective counting, it is worth documenting the quantification of the FRAG and P/(P + B) using photographs from different samples (Fig. 7). Sample 1209A-14H-1, 12 cm (134.32 rmcd) is light colored (White, 2.5Y 8/1) with high carbonate content (94%). Counts based only on the field of view of the photograph yields a FRAG of 18% and P/(P + B) of 0.96. Sample 1209A-14H-1, 53 cm (134.73 rmcd) is also light colored (White, 2.5Y 8/1) with high carbonate content (94%), having a FRAG of 23% and P/(P + B) of 0.95 (based on counts only from the field of view shown in the photograph). By contrast, sample 1209A-15H-7 W, 23.5 cm (153.10 rmcd) is dark (Gray, 2.5Y 4/1), with a low carbonate content (73%), and having a FRAG of 32% and P/(P + B) of 0.67.

4. Results

4.1. Stable isotopes

The $\delta^{13}C$ of bulk sediment varies from 0.54‰ to 3.20‰ across the studied interval (Supplemental Table 2, Fig. 8). The lowest and highest values are found at 210.76 and 219.89 rmcd, respectively. The $\delta^{13}C$ record begins with a prominent negative carbon isotope excursion (CIE) of ~2.7‰ between 219.8 and 217.8 rmcd, followed by a long-term low in $\delta^{13}C$, between 210 and 198 rmcd. Between 200 and 196 rmcd, there is a gradual positive shift in δ13C of nominally ~1.0‰. This record also indicates the presence of several significant $\delta^{13}C$ changes over relatively small changes in depth. Additional CIEs of 0.25 to 0.75‰ are present between 215 and 190 rmcd. Sediments above 185 rmcd display less variation in $\delta^{13}C$ but with several apparent cycles and a few minima, such as a marked low at 171.23 rmcd. Interestingly, only a relatively minor CIE of ~0.5‰ marks the prominent dark colored horizon at ~153 rmcd. Towards the top of the studied record, a significant increase in $\delta^{13}C$, from 1.15‰ to 1.89‰, occurs between 141 m and 138 rmcd.

The $\delta^{18}O$ values of bulk sediment vary from −1.67‰ to 0.93‰ (Fig. 8). The minimum and maximum values occur at 197.5 and 170 rmcd, respectively. Overall, values increase up the section and with greater variability compared to changes in $\delta^{13}C$. Though $\delta^{18}O$ and $\delta^{13}C$ exhibit only a weak positive correlation ($r^2 = 0.15$) considering the entire dataset (Fig. 10A), most of the significant negative CIEs correspond to drops in $\delta^{18}O$. Additionally, the positive shift in $\delta^{13}C$ between 141 and 138 rmcd correlates with an increase in $\delta^{18}O$. At a basic level, changes in the two stable isotope records track each other much more across short intervals than on the broad scale (Supplementary Table 4).

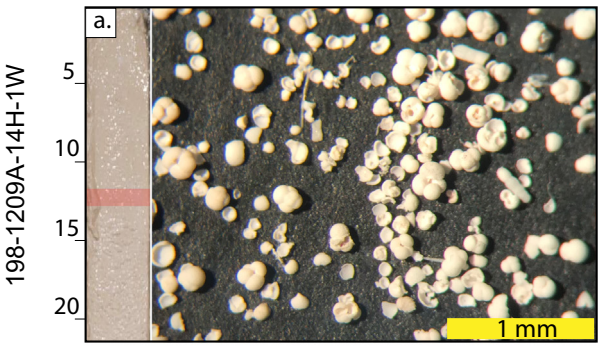

Counts: Whole forams (w)=52; Fragments (f)=101; Benthic forams (b)=2
Values: **Frag**= 18%; **P/P+B**=0.96

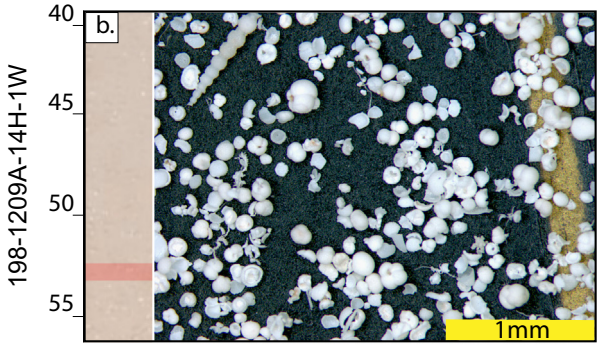

Counts: Whole forams (w)=90; Fragments (f)=225; Benthic forams (b)=4
Values: **Frag**= 23%; **P/P+B**=0.95

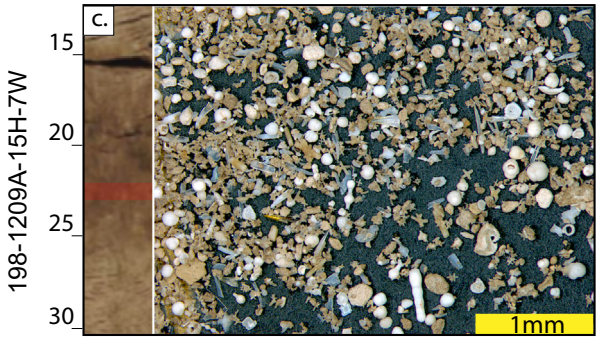

Counts: Whole forams (w)=42; Fragments (f)=169; Benthic forams (b)=20
Values:**Frag**= 33%; **P/P+B**=0.67

Fig. 7. Examples of different samples of high and low carbonate contents exhibiting different values of dissolution indices-FRAG and P/P + B. a. and b. Examples of samples 198-1209A-14H-1W-12cm and 198-1209A-14H-1W-53 cm with high carbonate content (>90%) have low number of fragments and high number of planktic foraminifers relative to benthic foraminifers, thus exhibiting low dissolution. c. Example of a sample (198-1209A-15H-7W-23 cm) with low carbonate content (<60%) exhibits high number of fragments, and low number of planktic foraminifers relative to benthic foraminifers, thus showing signs of high dissolution. Counts mentioned here are based solely on the field of view shown in the photograph, and differs from actual results, which are based on many more counts. This image is to demonstrate how methods were applied in FRAG and P/P + B calculations.

4.2. Carbonate content and mass accumulation rate

All samples have a carbonate content ranging between 50 and 100% (Fig. 9, Supplemental Table 1). The maximum and minimum values are ~99 wt% at 172.74 and 52.3 wt% at 153.04 rmcd, respectively. Except for some intervals, though, most samples yield carbonate contents exceeding 90 wt%. Indeed, the average carbonate content across all 333 measured samples is 92.3 wt%. Although precise comparisons are not possible (because of slightly different depth and sample heterogeneity), carbonate content values and ranges are consistent with previous data at much lower resolution (Fig. 9; Hancock and Dickens, 2005).

Carbonate content shows a modest negative correlation ($r^2 = 0.45$) with magnetic susceptibility (MS) (Fig. 10B). Such correlation improves when one considers only samples with carbonate content ≤90% (Fig. 4, Supplementary Table 4). Considering all 333 samples, carbonate content shows almost no correlation with $\delta^{13}C$ (Fig. 10C), which improves to 0.15 considering only the small subset of data.

Across the examined section, carbonate mass accumulation rate (MAR_{carb}) averages 0.73 g/cm^2/ky. MAR_{carb} at each sampled interval is dependent on calculation of SR and carbonate content of the interval (Eqn 2). The maximum and minimum values of MAR_{carb} are 1.35 g/cm^2/ky at 194.87 rmcd and 0.16 g/cm^2/ky at 153.04 rmcd, respectively. Between 220 and 205 rmcd, average MAR_{carb} is ~0.31 g/cm^2/ky, and increases to an average of ~0.95 g/cm^2/ky between 205 and 155 rmcd, and again drops to ~0.39 g/cm^2/ky above 155 rmcd (Fig. 9).

4.3. Scanning electron microscope work

Representative FESEM images show foraminifers and fragments (Fig. 6). Other than enabling a better description on methods for measuring dissolution proxies, such imaging highlights two points. Foraminifers are often recrystallized and secondary calcite exists in the sediments (Supplemental Fig. S2). Such recrystallization can particularly affect $\delta^{18}O$, given high water/grain ratios in sediment, geothermal gradients and a strong temperature effect on oxygen isotope fractionation (Lohmann, 1995; Schrag, 1999). SEM imagery also emphasizes on the highly heterogeneous nature of Eocene sediments at Site 1209, even across small depth increments.

4.4. Planktic foraminiferal fragmentation

The record of planktic foraminiferal fragmentation, measured as FRAG (%) shows high variability. Across the studied section, FRAG varies between 1.1 and 47.3%, and averages 14% (Fig. 8, Supplemental Table 3).

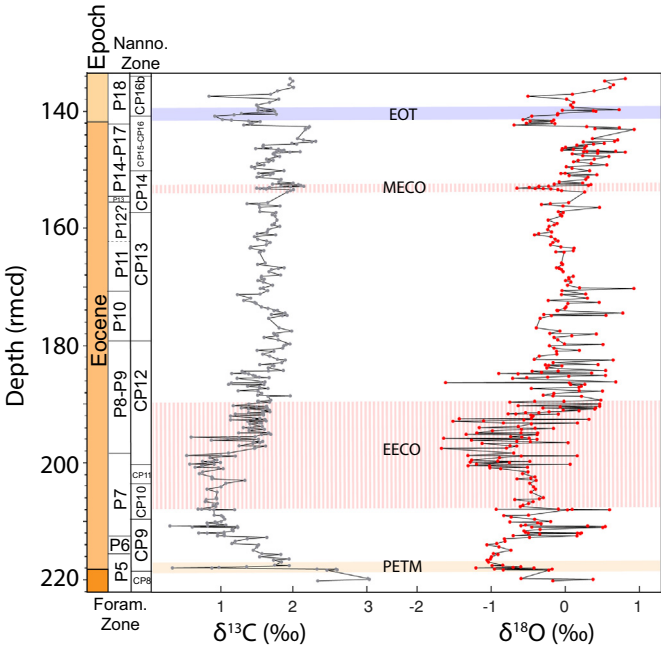

Fig. 8. Results of bulk carbonate isotope analysis of sediments from Site 1209. Changes of $\delta^{13}C$ and $\delta^{18}O$ of bulk carbonates in samples of Site 1209 are plotted against depth (rmcd).

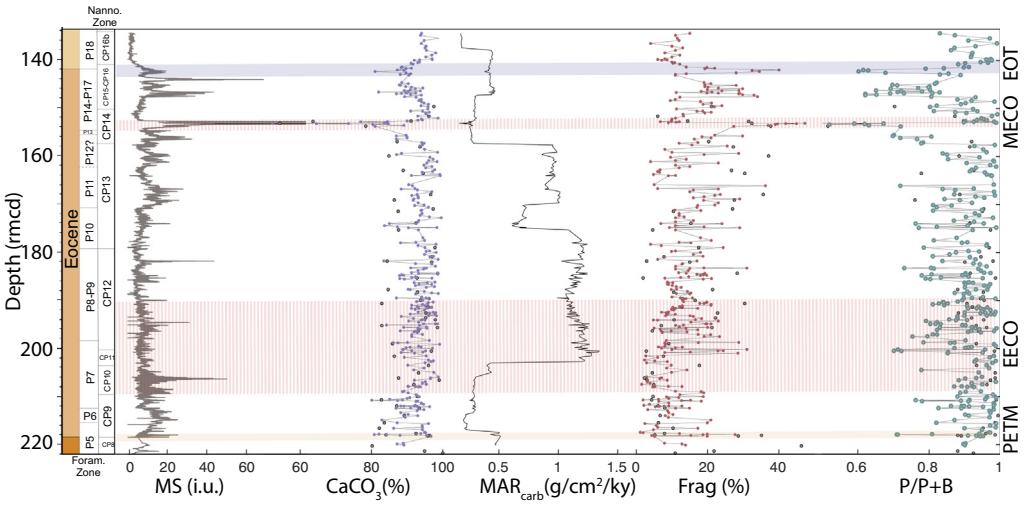

Fig. 9. Results of dissolution indices of sediments from Site 1209. Changes of MS (Bralower et al., 2002), carbonate content ($CaCO_3$%), carbonate mass accumulation rate (MAR_{carb}), fragmentation index (FRAG %) and planktic to benthic foraminiferal ratio (P/P + B) are plotted against depth (rmcd). Data from Hancock and Dickens (2005) have also been plotted as grey solid circles, in the panels of $CaCO_3$%, FRAG % and P/P + B.

The minimum value occurs at 217.46 rmcd, while the maximum value occurs at 153.04 rmcd, and at the depth of lowest carbonate content. In the interval above 160 rmcd, FRAG is persistently higher than the section below. This trend is similar to a previously published low resolution dataset from Site 1209 (Fig. 9, Hancock and Dickens, 2005).

FRAG shows a weak negative correlation with carbonate content, with a $r^2 = 0.22$ for our dataset. This is somewhat different than previous observations at Site 1209 (Hancock and Dickens, 2005), where no correlation was found (Fig. 10D). Between FRAG % and $\delta^{13}C$, there again appears to be almost no correlation (Fig. 10E). However, it is important to note that, across short intervals of high MS and low carbonate contents (e.g., at ~218 and ~ 153 rmcd), high FRAG values occur (Fig. 9). Above 140 rmcd, when MS drops and carbonate content increases, FRAG exhibits a decreasing trend. In summary, a good correlation between FRAG, carbonate content and MS occurs across certain specific intervals, but becomes minimized when taking the entire dataset into account (Supplementary Table 4).

4.5. Planktic to benthic foraminiferal ratio

The P/P + B ratio ranges between 0.41 and 0.99, and average 0.88 (Fig. 9, Supplemental Table 3). The maximum value occurs at 136.42 rmcd, while the minimum value again occurs at 153.04 rmcd. In past work at Site 1209 (Hancock and Dickens, 2005), data was presented as BENTH, where:

$$\text{BENTH}\ (\%) = \text{B}/(\text{P} + \text{B}) * 100 \quad (5)$$

Such data can readily be converted to P/P + B ratio as:

$$\text{P}/\text{P} + \text{B} = (\text{BENTH}\ (\%)/100) - 1 \quad (6)$$

Records of the P/P + B ratio from both studies again show similarities across Eocene sediment (Fig. 9). The P/P + B record shows a drastic decrease above 160 rmcd, which coincides with the major increase of FRAG. Similar to FRAG, P/P + B exhibits high scatter across short changes in depth.

The planktic/benthic index shows a weak negative correlation with carbonate content, with a $r^2 = 0.22$ for our entire dataset (Fig. 10F). This is similar to that reported previously (Hancock and Dickens, 2005). Like FRAG %, P/(P + B) shows almost no correlation with $\delta^{13}C$ (Fig. 10G). But, FRAG % and P/P + B have relatively good negative correlation between themselves; $r^2 = 0.61$ (Fig. 10H). Such values of correlation can again change significantly when short intervals are considered. For example, at ~218 and ~153 rmcd, distinct decreases in carbonate content, increases in MS and FRAG coincide with decreases in P/(P + B). Also above 140 rmcd, when FRAG decreases, P/(P + B) increases, and such changes are consistent with changes in carbonate content and MS. The overall scatter in the data often dilutes such correlation across short intervals, as seen by improved r^2 for the selected subset of data (Supplementary Table 4).

5. Discussion

5.1. Bulk isotope records across the Eocene

5.1.1. General recognition

Bulk carbonate comprises various components, each with potentially distinct carbon and oxygen isotope compositions because of different fractionation, habitat or post-depositional modification. Interpreting bulk isotope records necessarily carries complications, especially if fractionation factors or the relative abundance of different components vary over time. Sediments from Site 1209 mostly consist of nannofossil ooze (Bralower et al., 2002; Hancock and Dickens, 2005; Westerhold et al., 2018), so the bulk carbonate isotope records should largely reflect the average composition of this fine fraction, which originally formed in the overlying photic zone. As implied by the "ooze" description, significant lithification of sediments has not occurred at Site 1209, and post-depositional alteration in isotope compositions might be low. However, evidence of secondary overgrowth on foraminifers and presence of authigenic calcite (Supplemental Fig S1; Dutton et al., 2005) indicates some recrystallization. Because of much lower water/rock ratios for carbon and because of smaller temperature-related fractionation for carbon isotopes, recrystallization generally affects $\delta^{13}C$ much less than $\delta^{18}O$ (Romanek et al., 1992; Sexton et al., 2006; Blanchet et al., 2012; Edgar et al., 2015).

5.1.2. Carbon isotopes

The record of bulk carbonate $\delta^{13}C$ at Site 1209 (Figs. 8, 11) exhibits significant variations over short time increments. This does not originate from misaligned cores or analytical error, but represents the short-term variability within samples. Over some intervals, changes in $\delta^{13}C$ directly relate to variations in carbonate content and MS (Fig. 4). Notably, the high-resolution early Eocene bulk $\delta^{13}C$ record at adjacent Site 577 (Fig. 11) shows similar short-term changes.

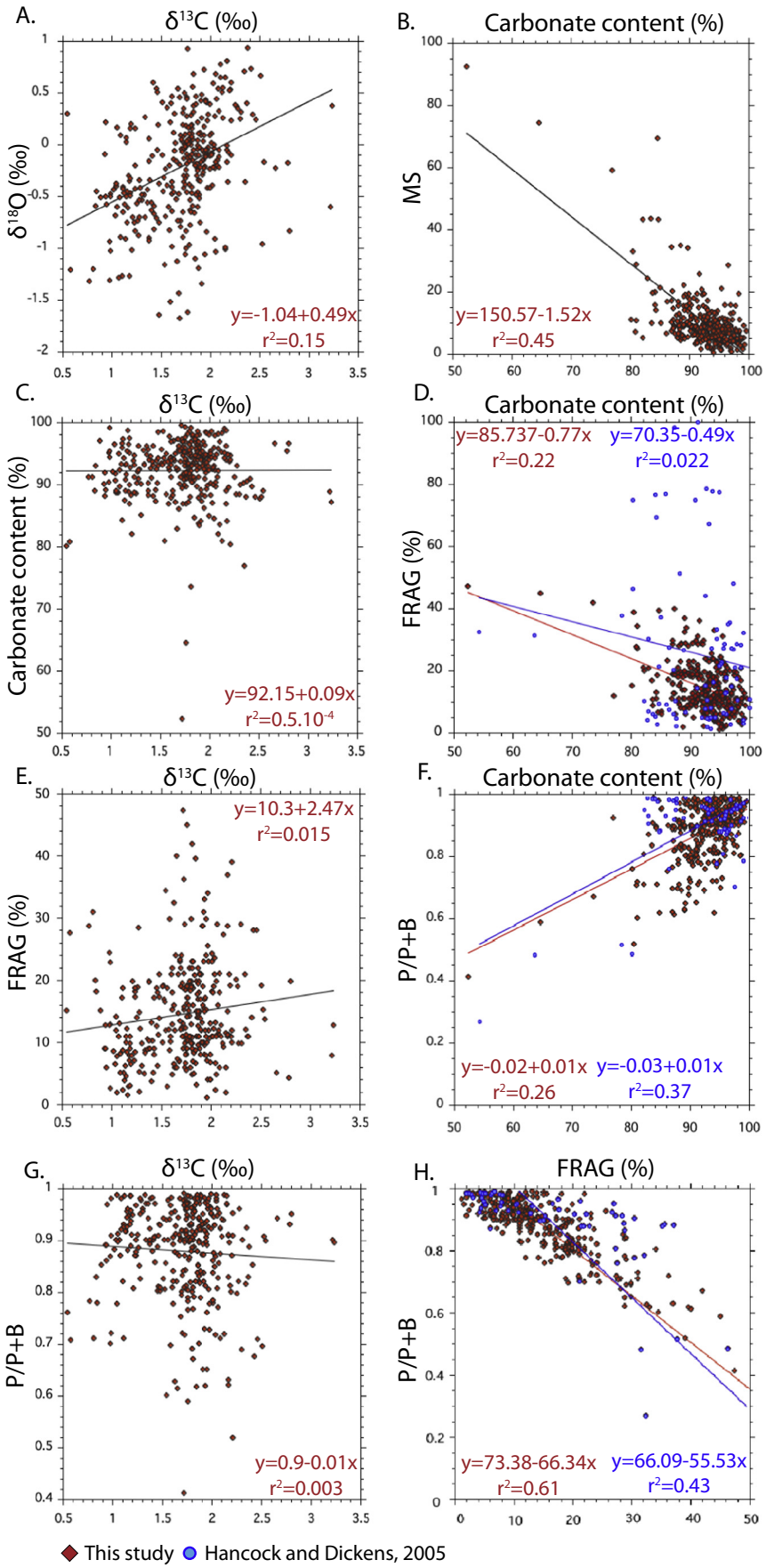

Fig. 10. Cross plots showing r^2 values between proxies across the entire dataset. The bivariate plots show correlation between FRAG, P/P + B, $CaCO_3$%, MS, $\delta^{13}C$ ‰ and $\delta^{18}O$ ‰. Data from Hancock and Dickens (2005) have also been plotted where available.

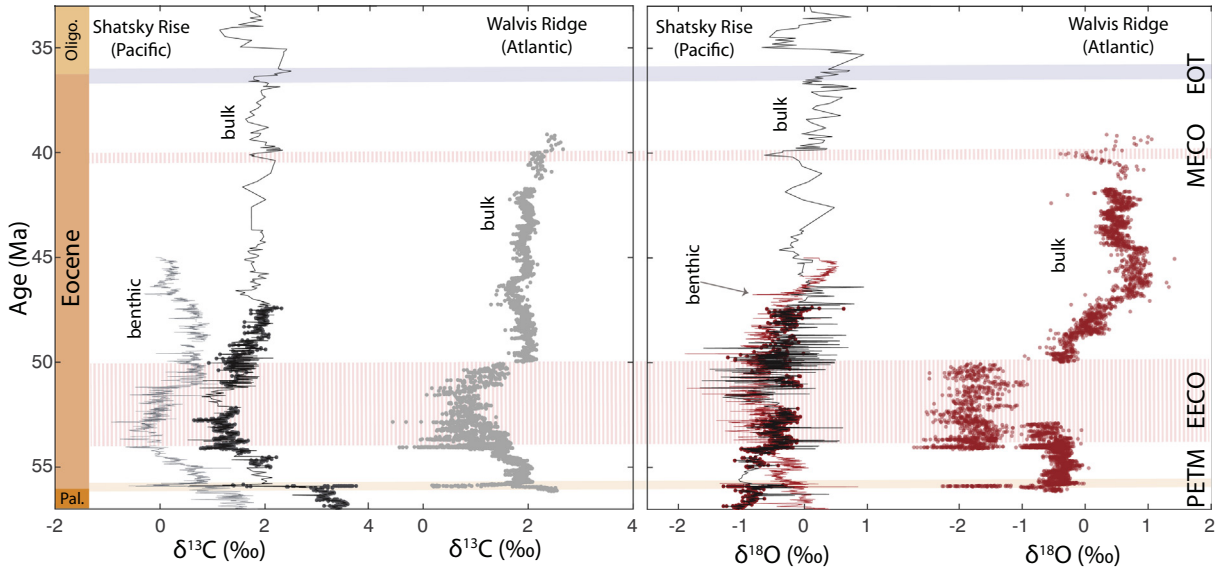

Fig. 11. Eocene isotope stratigraphy at Shatsky Rise (north-central Pacific) and Walvis Ridge (south Atlantic). Bulk carbonate $\delta^{13}C$ and $\delta^{18}O$ record from Shatsky Rise comprises data from present study on Site 1209 marked by solid black line and from nearby Site 577 represented by solid dots on the black line (Dickens and Backman, 2013; Luciani et al., 2016). Benthic foraminiferal isotope data measured on *Nuttalides truempyi* from Site 1209 (Westerhold et al., 2018) is plotted alongside the bulk isotope record, represented by grey line for $\delta^{13}C$ and red line for $\delta^{18}O$. A composite bulk carbonate isotope record from multiple sites on Walvis Ridge (Kelly et al., 2010; Zachos et al., 2010; Boscolo Galazzo et al., 2014; Kirtland Turner et al., 2014; Lauretano et al., 2016; Westerhold et al., 2017), marked by a dotted (grey for $\delta^{13}C$ and red for $\delta^{18}O$) line is also shown beside the Shatsky Rise isotope record. (For interpretation of the references to color in this figure legend, the reader is referred to the web version of this article.)

Our study extends the existing early Eocene bulk carbonate $\delta^{13}C$ record from Site 577 (Fig. 3; Shackleton et al., 1985; Dickens and Backman, 2013; Luciani et al., 2016) across the entire Eocene. Despite differences in sample resolution, the new record from Site 1209 fits well with the existing early Eocene record from Site 577 (Figs. 11), presumably because of geographical proximity and similar paleodepth (Fig. 3). At least between 56 and 45 Ma, the bulk $\delta^{13}C$ record at Site 1209 also tracks the benthic foraminiferal $\delta^{13}C$ record at this location (Westerhold et al., 2018) (Fig. 11). A consistent offset of 1–2‰ exists, because bulk carbonate at Sites 1209 and 577, dominated by calcareous nannofossils but with significant planktic foraminifers, mostly represents upper water column values. Such an offset is also noted in Neogene carbonates from equatorial Pacific (Reghellin et al., 2020).

Comparison of the bulk $\delta^{13}C$ record from Shatsky Rise to similar records elsewhere is limited because of the lack of continuous Eocene bulk $\delta^{13}C$ records from other open ocean sites. Several long- and short-term changes in bulk $\delta^{13}C$ at Site 1209 appear to track those at Walvis Ridge, in the south Atlantic (Fig. 11; Westerhold et al., 2017). As the records derive from different carbonate components in different ocean basins, the similarities likely reflect past changes in the $\delta^{13}C$ composition of the ocean-atmosphere system.

A long-term depletion in $\delta^{13}C$, which began in the late Paleocene, terminates at ~53 Ma and the start of the EECO. About halfway through EECO, after ~52 Ma, a major (~0.8‰) positive shift in $\delta^{13}C$ occurred (Fig. 11; Kirtland Turner et al., 2014; Luciani et al., 2016; Westerhold et al., 2018). However, following this positive shift, especially after 48 Ma, both bulk and benthic foraminiferal $\delta^{13}C$ records show minimal long-term variance until the end of the Eocene. Given long-term warming towards EECO and long-term cooling after EECO (Figs. 1; 11; Zachos et al., 2001; Bijl et al., 2009; Crouch et al., 2020), coupling of global temperature and carbon cycling appear to change significantly within the early Eocene. Specifically, potential changes in ocean-atmosphere carbon mass before and during EECO relate to changes in carbon fluxes with very different $\delta^{13}C$ than that of the exogenic carbon cycle, whereas those after EECO had similar $\delta^{13}C$ to that of the exogenic carbon cycle.

As recognized for over a decade, a series of significant short-term negative CIEs occurred during the early Eocene (e.g. Nicolo et al., 2007; Zachos et al., 2010). Some of these clearly relate to "hyperthermal events" (Lourens et al., 2005; Agnini et al., 2009; Lauretano et al., 2015), and are apparent in the bulk $\delta^{13}C$ records at Sites 577 and 1209, as for example a 2.5‰ drop in $\delta^{13}C$ marking PETM, a 1‰ and 0.5‰ marking H-1/ETM2 and J events respectively. Multiple CIEs between 53 and 50 Ma characterize EECO (Luciani et al., 2016; Westerhold et al., 2018). However the interval following 48 Ma is far less studied and not well constrained both in terms of isotope stratigraphy as well as deep-sea carbonate accumulation.

Significant deep-sea carbonate dissolution marks the main early Eocene hyperthermal events (Dickens et al., 1997; Stap et al., 2009), often accompanied by a drop in carbonate content and spike in MS. Given a limited totality of samples, and a decrease in sedimentation rates (Fig. 5) after 48 Ma, we thus specifically collected samples spanning MS spikes at Site 1209 (Fig. 4), assuming they might represent additional hyperthermals. Our study documents a number of such intervals with low carbonate content, high MS and a drop in $\delta^{13}C$ (Fig. 12). A very significant decrease in carbonate content and increase in MS occurs at ~40.5 Ma, accompanied by a negative CIE of ~0.4‰. This is corresponding to MECO, a prominent global warming event of middle Eocene (Bohaty and Zachos, 2003; Bohaty et al., 2009; Sluijs et al., 2013). Some other negative CIEs during middle-late Eocene can be identified in our record at ~41.5 Ma, ~36.5 Ma and ~ 35.5 Ma (Fig. 12). These middle-late Eocene CIEs, smaller in magnitude than the hyperthermals of early Eocene, are superimposed on a rather 'flat' long-term trend in bulk $\delta^{13}C$ curve.

A prominent positive shift in $\delta^{13}C$ occurs between 34 and 33 Ma, at the Eocene-Oligocene transition. This is known from other records and thought to be associated with major global cooling, Antarctic glaciation, sea level drop and decrease in shelf carbonate burial (Coxall et al., 2005; Merico et al., 2008; Armstrong McKay et al., 2016).

5.1.3. Oxygen isotopes

Like the bulk $\delta^{13}C$ record, the bulk $\delta^{18}O$ record at Site 1209 shows significant variations across small depth/time intervals. However, the amplitude of variation is much greater (Fig. 11). One reason for such variations could be post-burial recrystallization of calcite, which can significantly affect bulk $\delta^{18}O$ (Lohmann, 1995; Schrag, 1999). Secondary calcite formation from partial dissolution of foraminiferal tests, which

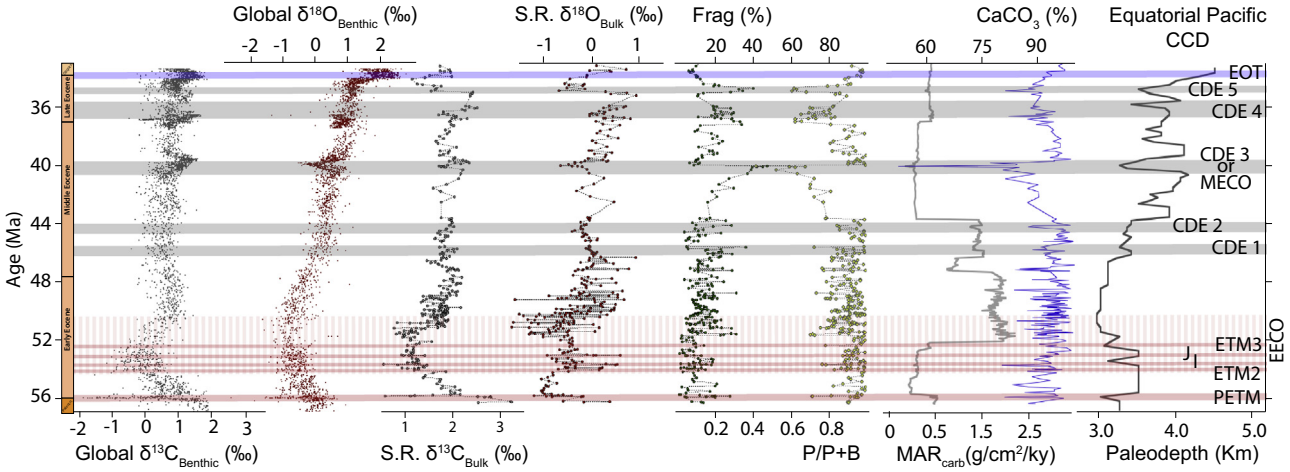

Fig. 12. The Eocene isotope stratigraphy, record of carbonate preservation at Shatsky Rise (S.R.) and the equatorial Pacific CCD. Bulk carbonate $\delta^{13}C$ and $\delta^{18}O$ record from Site 1209 are tied with dissolution proxies (FRAG and P/P + B), carbonate content and carbonate mass accumulation rate. Global benthic foraminiferal stack (Cramer et al., 2009) and equatorial Pacific CCD reconstruction (Pälike et al., 2012) are also shown alongside the record from Shatsky Rise. Red lines represent the early Eocene hyperthermals, while grey line denote high amplitude variations in carbonate dissolution during middle-late Eocene, referred to as carbonate dissolution events (CDEs), numbered 1–5, which are synchronous with CCD fluctuations of equatorial Pacific. CDE 3 is same as MECO. (For interpretation of the references to color in this figure legend, the reader is referred to the web version of this article.)

is evident in samples from Site 1209 (Supplemental Fig. S2), could sometimes result in heavier $\delta^{18}O$ values of altered foraminiferal tests (Pearson et al., 2001; Sexton et al., 2006). However, the actual amount of diagenetic alteration of the bulk sediments is hard to assess, as it depends on multiple factors, such as time, burial depth and the local geotherm (Schrag et al., 1995). Hence, the bulk sediment $\delta^{18}O$ record at Site 1209 does not appear ideal for palaeoceanographic interpretations. Despite this, some trends and deviations probably are directly related to changes in sea surface temperature.

Between 57 and 54 Ma, the bulk $\delta^{18}O$ record is lower than the benthic foraminiferal $\delta^{18}O$ record, both globally and at Site 1209, by about 1–1.5‰ (Fig. 11). Such a difference may reflect a thermally stratified ocean, where surface waters are warmer than deep waters. However, during the rest of the early Eocene (~54–48 Ma), the offset is rather negligible; by comparison, the difference between bulk carbonate and benthic foraminiferal $\delta^{18}O$ is about 3–4‰ in upper Miocene through Holocene of the tropical Pacific (Reghellin et al., 2020). Moreover, between 53 and 50 Ma, which corresponds to the EECO, there is a general low in bulk $\delta^{18}O$. While somewhat consistent with bulk $\delta^{18}O$ records from sites on Walvis Ridge (Westerhold et al., 2017), and with extreme warmth during the EECO, values drop to those of benthic foraminifers, which is difficult to explain. After the termination of EECO, $\delta^{18}O$ records at Site 1209 and at Walvis Ridge exhibit an increasing trend (Fig. 11). This possibly signals the beginning of long-term Eocene cooling. However, between 45 and 41 Ma, sedimentation rate drops sharply at Site 1209 (Fig. 5), so that it is difficult to precisely constrain details at the current sampling resolution. After the termination of MECO and through the rest of middle and late Eocene, there again is a long-term increasing trend in $\delta^{18}O$, consistent with cooling heading towards the Eocene-Oligocene transition.

Compiled bulk $\delta^{18}O$ data from Sites 1209 and 577 (Fig. 11) shows a prominent negative excursion of >1‰ corresponding to the PETM. This is also found in bulk carbonate $\delta^{18}O$ records from other locations (Leon-Rodriguez and Dickens, 2010; Slotnick et al., 2015; Agnini et al., 2016) and benthic $\delta^{18}O$ records (Zachos et al., 2001, 2008; Westerhold et al., 2018). Multiple negative oxygen isotope excursions occur between 54 and 50 Ma, including the H1/ETM2 and J events at ~54 Ma and ~53 Ma, respectively. Another prominent (~1‰) negative $\delta^{18}O$ excursion occurs between 40.5 and 40 Ma, likely corresponding to the MECO (Bohaty and Zachos, 2003; Sluijs et al., 2013; Boscolo Galazzo et al., 2014). A significant (~2‰) positive excursion in bulk $\delta^{18}O$ occurs between 34 and 33 Ma, which marks the Eocene-Oligocene transition, global cooling and first polar ice growth of the Cenozoic (Zachos et al., 2001; Coxall et al., 2005; Carter et al., 2017).

5.2. Carbonate dissolution at Site 1209

5.2.1. General features in carbonate accumulation records

Many open ocean sites at low-latitude, especially on bathymetric highs, have two main inputs raining from surface water: biogenic carbonate and wind-blown terrigenous material. Amongst such sites without significant biogenic silica, the lysocline has been defined as the water depth where seafloor carbonate content drops below 80% (Boudreau et al., 2010). By this criteria, Site 1209 lay about the lysocline depth (Fig. 2) throughout much of the Eocene (Bralower et al., 2002). However, carbonate preservation is subtler than this.

Carbonate content of deep-sea and siliceous-poor sediments is generally inversely related to MS, because the non-carbonate fraction carries almost all the magnetic signal (Ellwood et al., 2000; Lourens et al., 2005; Leon-Rodriguez and Dickens, 2010). Numerous intervals at Site 1209 with carbonate content below 80% have relatively high MS, high FRAG and low P/(P + B) (Fig. 12). One such interval, associated with a drop in MAR_{carb}, occurred at ~56 Ma and corresponds to the PETM, an event related to intense worldwide ocean acidification (e.g. Dickens et al., 1997; Zachos et al., 2005; Penman et al., 2014) (Fig. 12). A similar response happened across other intervals between 54 and 50 Ma, notably including the H-1/ETM-2, I, J and K/X/ETM-3 events (Fig. 12). This is consistent with the idea that multiple early Eocene hyperthermals were associated with intense ocean acidification and short-term shoaling of the CCD and lysocline (e.g. Zachos et al., 2008; Leon-Rodriguez and Dickens, 2010; Slotnick et al., 2015; Lauretano et al., 2016). At a simple level, the short-term hyperthermal events represent times of increased carbonate dissolution on the seafloor (Hancock and Dickens, 2005; Leon-Rodriguez and Dickens, 2010; Zachos et al., 2010) and when the lysocline shoaled above the depth of Site 1209 (Fig. 2).

Readily clear, however, many samples at Site 1209 do not display expected strong relationships between $CaCO_3$%, MS, FRAG and P/(P + B). Indeed, considering the entire suite of samples, bivariate plots demonstrate relatively low correlations between some of these parameters (Fig. 10).

Here it is important to compare carbonate content and dissolution proxies in the current study with those in the previous work at Site 1209 (Hancock and Dickens, 2005). The r^2 value between carbonate content and FRAG is significantly higher for the present dataset

(Fig. 10D). Between carbonate content and P/(P + B), difference in r^2 values between the two studies is much lower (Fig. 10F). At least three reasons can explain such differences. First, the difference in sample numbers examined in the two studies can contribute to differences in r^2. Second, the sampled intervals are not exactly the same, sediment heterogeneity at the cm-scale can result in variability of FRAG and P(/P + B) values. Third, the methods are somewhat different, especially for FRAG. Following Leon-Rodriguez and Dickens (2010), tests that show significant peeling are also considered fragments. Though quantitative, the dissolution indices largely depend on sample heterogeneity and subjectivity.

Furthermore, the relationship between carbonate content and dissolution indices is not straightforward (Hancock and Dickens, 2005). As noted, planktic foraminifers dissolve more readily than benthic foraminifers and calcareous nannofossils (Berger, 1973; Reghellin et al., 2020; D'Onofrio et al., 2020). For sediments dominated by calcareous nannofossils, modest dissolution can therefore result in a relatively minor drop in $CaCO_3$ but relatively high FRAG and low P/(P + B). This concept is particularly relevant to deep-sea sections, where open ocean carbonate accumulation occurred near the lysocline. That stated, drops in carbonate accumulation should characterize such intervals. Despite complexities, all information at Site 1209 suggests a first-order increase in carbonate dissolution that began ca 44 Ma.

Shatsky Rise presumably experienced limited subsidence after the Cretaceous (Bralower et al., 2002), given its Jurassic age. With this assumption, records of carbonate accumulation and preservation can be placed within the context of fixed water depth across the Paleogene.

5.2.2. Carbonate dissolution in early Eocene

During early Eocene, various proxies suggest relatively low carbonate dissolution at Site 1209 (Fig. 12), which somewhat contrasts and complicates views from previous work at sites examined elsewhere (Hancock et al., 2007; Zachos et al., 2010; Leon-Rodriguez and Dickens, 2010; Pälike et al., 2012; Slotnick et al., 2015). The overall low MAR of carbonate, between the PETM and the K/X/ETM-3 events, may result in part from inclusive hyperthermals. Presumably, this time represents accelerated long-term inputs of carbon to the ocean, which also drove the associated overall decrease in global exogenic $\delta^{13}C$ (Komar et al., 2013). An explanation for lowered overall carbonate MAR is that multiple prominent short-term dissolution horizons linked to the hyperthermals (noted above) significantly decreased million-year carbonate accumulation.

Like previous work at Site 1209 (Hancock and Dickens, 2005), a subtle but detectable increase in carbonate dissolution begins about halfway through EECO at ~52 Ma (Fig. 12). This is approximately when $\delta^{13}C$ records at Shatsky Rise and elsewhere show a pronounced rise (Kirtland Turner et al., 2014; Luciani et al., 2016; Westerhold et al., 2018), and consistent with lowered long-term fluxes in carbon inputs and a rise in carbonate saturation horizons (Slotnick et al., 2015). A recent study by D'Onofrio et al. (2020) has documented a similar observation at Site 1258 in the Atlantic, where an increase in the baseline of fragmentation was recorded in the upper part of early Eocene sediment sequences.

A more perplexing problem at Site 1209 is a relatively high carbonate accumulation that persists from 52 to 48 Ma and until after the EECO (Fig. 12). During the same time at other deep-sea locations, carbonate saturation horizon rose significantly (Pälike et al., 2012). It is not an issue of erroneous ages, because the $\delta^{13}C$ records at Site 1209 would not otherwise align with sites elsewhere (Fig. 11). It is possible that the CCD and lysocline at Shatsky Rise were deeper than those at equatorial Pacific sites, perhaps signaling a shift in the location of carbonate accumulation and the flattening of latitudinal carbonate dissolution horizons. Relatively high nannofossil productivity during this interval may have driven the higher carbonate MAR, as coarse fraction abundances at Site 1209 appear to be low during this interval (Hancock and Dickens, 2005; Westerhold et al., 2018).

5.2.3. Middle-late Eocene carbonate dissolution events

After 44 Ma, Site 1209 shows lowered carbonate MAR and overall greater carbonate dissolution (Fig. 12). A drop in sedimentation rate is evident especially after 44 Ma (Fig. 5), which results in a lower temporal resolution for data across the middle and late Eocene. Several episodes of intense carbonate dissolution are recorded at Site 1209 (Fig. 12), which we refer to as carbonate dissolution events (CDEs). These fluctuations possibly relate to changing carbonate budget in middle-late Eocene Pacific waters (Hancock and Dickens, 2005). At least seven high amplitude fluctuations in CCD have been reported previously from equatorial Pacific sediments that accumulated between 45 and 34 Ma (Pälike et al., 2012). The CDEs at Site 1209 appear to be synchronous with the variations in the equatorial Pacific CCD (Fig. 12). This implies that fluctuations in carbonate saturation horizons over the middle-late Eocene may have been widespread.

5.2.4. A potential problem with tectonics

Long-term changes in carbonate dissolution at Site 1209 (Fig. 12), especially the increase after 44 Ma, could relate to subsidence. This speculation arises because a major tectonic reorganization occurred within the western Pacific between the late-early Eocene and early-middle Eocene (O'Connor et al., 2015; Sutherland et al., 2020), and because vertical movements of the seafloor would result in apparent changes of saturation horizons (Fig. 2). A change in Shatsky Rise water depth between Cretaceous-early Eocene and late Eocene-Neogene has been suggested previously (Ito and Clift, 1998). We cannot exclude potential tectonic effects on the Site 1209 dissolution records in the background. Importantly, though, the short-term and significant intervals of carbonate dissolution at Site 1209 are almost assuredly related to changes in regional to global carbon cycling.

5.3. Comparison of early Eocene hyperthermals and short-term events of middle-late Eocene

The term hyperthermal generally refers to extreme short-term (<200 kyr) global warming events that occurred during the latest Paleocene and early Eocene. Notably, these events are marked by prominent negative $\delta^{13}C$ excursions (CIEs) and seafloor carbonate dissolution (Sluijs et al., 2009; Littler et al., 2014; Lauretano et al., 2016). At Site 1209, our study has identified the PETM, H-1/ETM2, I, J and the end part of K/X or ETM3. These hyperthermals exhibit CIEs and carbonate dissolution (Fig. 12). Of more novel interest, significant increases in carbonate dissolution exist at Site 1209 across at least five middle-late Eocene intervals (Fig. 12), marked as carbonate dissolution events (CDEs) 1 through 5.

The most significant carbonate dissolution happened at ~40.5 Ma, and corresponds to MECO. Such seafloor dissolution has been documented in other ocean basins (e.g. Henehan et al., 2020). Interestingly, at Site 1209, the intensity of dissolution at MECO exceeds that during the PETM and early Eocene hyperthermals. Moreover, as depicted by changes in benthic foraminiferal $\delta^{18}O$ (Fig. 1) and other proxies, the middle-late Eocene dissolution intervals occurred during an overall long-term cooling trend, whereas the early Eocene hyperthermal events occurred during a long-term warming trend. There are also differences in the background carbon cycle, as inferred from the long-term $\delta^{13}C$ records and variations in seafloor carbonate dissolution horizons (Figs. 11, 12), as the duration of hyperthermals was generally lesser than CDEs.

There is no a priori reason that all short-term dissolution horizons spanning the Eocene have a similar origin. Indeed, even across the early Eocene, ongoing debates continue as to whether the PETM indicates a special cause or represents the most profound example of similar process (e.g. Nicolo et al., 2007). To further assess the relation between CIEs and carbonate dissolution across short-term perturbations across the Eocene, we revisit correlations between various parameters using a different approach. For five major early Eocene

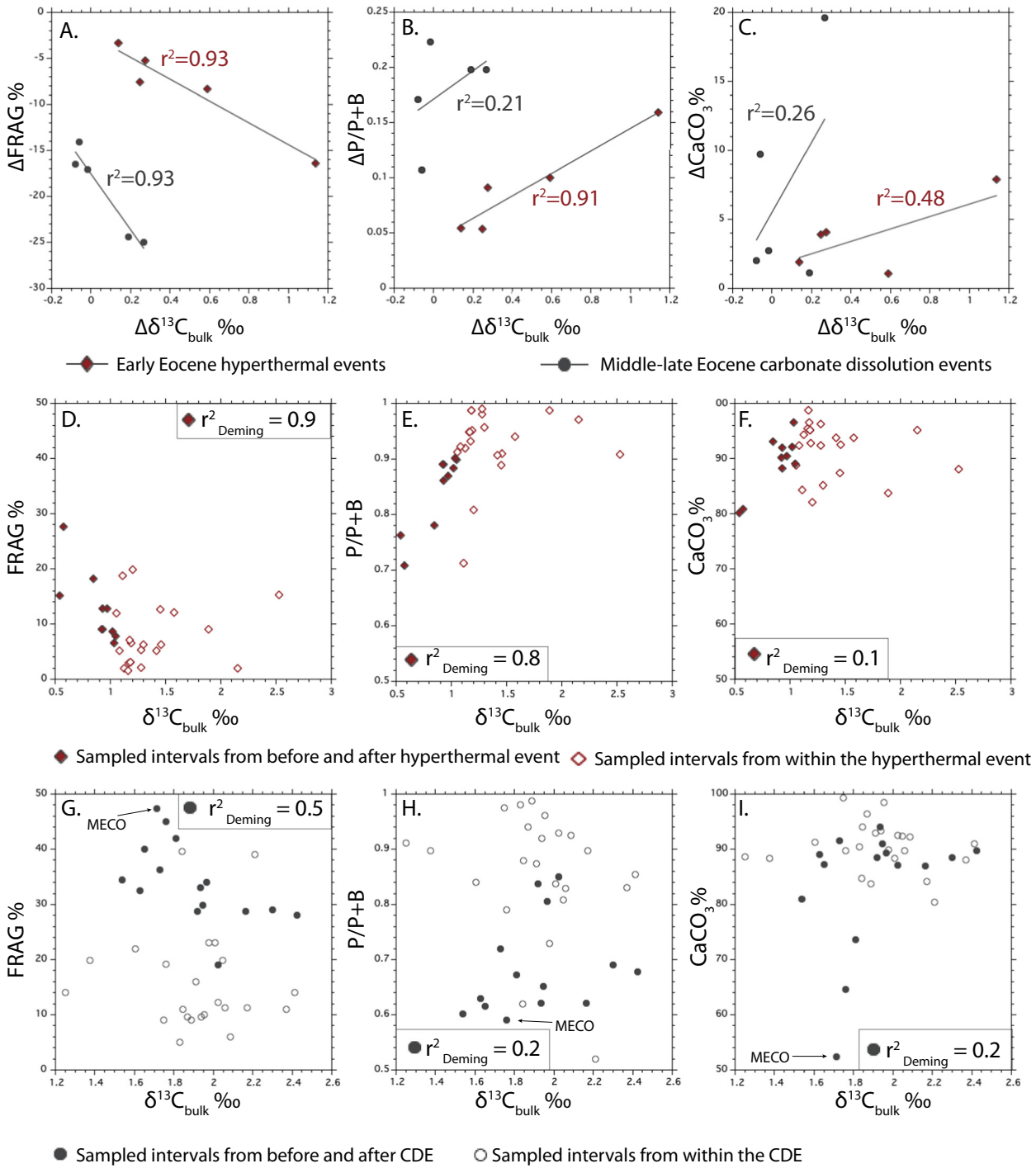

Fig. 13. Comparison of early Eocene hyperthermals and middle-late Eocene carbonate dissolution events. Cross plots A–C shows r^2 between Δ dissolution proxy (FRAG %, P/P + B, $CaCO_3$%) and Δ $\delta^{13}C$ for five hyperthermal events, in red and five carbonate dissolution events, in grey (intervals are marked in Fig. 12). Cross plots D-F directly shows proxy values from intervals within (marked by solid red rhombs) and just outside (open red rhombs) the hyperthermal events. Cross plots G-I directly shows proxy values from intervals within (marked by solid grey rhombs) and just outside (open grey rhombs) the intervals of carbonate dissolution events. MECO or CDE3 is also marked for reference. (For interpretation of the references to color in this figure legend, the reader is referred to the web version of this article.)

hyperthermals and for five major dissolution events of the middle-late Eocene, we calculate the change in a proxy (Δproxy) relative to "background" conditions as:

$$\Delta\text{proxy} = (\text{mean value of samples before and after an event}) - (\text{mean value of sample during the event}) \quad (7)$$

Such Δproxy values were calculated for FRAG, P/P + B, $CaCO_3$% and $\delta^{13}C$ (Fig. 13).

As previously noted, various parameters have rather poor correlation between each other over the entire dataset (Fig. 10). However, when examined using the above approach, a fundamental difference arises between different short-term events. In particular, over short increments, r^2 values, using linear regression methods, between $\delta^{13}C$ and dissolution proxies (e.g. ΔP/P + B versus Δ$\delta^{13}C$) are higher for early Eocene hyperthermals than for middle-late Eocene CDEs (Fig. 13). Similarly, using Deming regression methods, r^2 is generally higher for proxy relationships in case of early Eocene hyperthermals than the CDEs (Fig. 13,

Supplementary Table 5). The simplest explanation is that, during Early Eocene hyperthermals, elevated inputs of ^{13}C-depleted (organic-related) carbon into the ocean-atmosphere system drove seafloor carbonate dissolution (Dickens et al., 1997; Zachos et al., 2005; Zeebe et al., 2009). By contrast, the dissolution events of the middle-late Eocene were related to changing ocean carbonate budgets with either limited addition of carbon to the ocean-atmosphere system, or little difference between the $\delta^{13}C$ of extra carbon and the exogenic carbon cycle.

5.4. Dissolution in terms of global climate and carbon cycling

Changes in benthic foraminiferal $\delta^{18}O$ records (Fig. 11) and other proxy information (e.g. Dutton et al., 2005; Cramwinckel et al., 2018) strongly suggest long-term global warming heading into EECO and long-term cooling following this interval. These changes have been widely linked to variations in atmospheric pCO_2 (e.g. Zachos et al., 2008; Pagani et al., 2011; Pälike et al., 2012), although available proxy records for this parameter have high uncertainly (e.g. Royer et al., 2004; Beerling and Royer, 2011). Numerous records indicate major long-term changes in $\delta^{13}C$ before the ECCO, but no significant long-term trend in $\delta^{13}C$ following the interval (Fig. 11).

With simple views of global carbon cycling, variations in atmospheric pCO_2 should relate to net changes in carbon inputs and outputs to the ocean and atmosphere (e.g. Dickens, 1999; Komar et al., 2013). Crucial to a full understanding of climate and carbon cycling across the Cenozoic are records of deep-sea carbonate accumulation, as this is the dominant output of carbon from the ocean-atmosphere system.

In some regards, our records at Site 1209 support aspects of basic carbon cycle theory. The early Eocene hyperthermals manifest as negative CIEs along with transient increases in carbonate dissolution. Other than the broad and transient changes in the Early Eocene that have been discussed in previous works (e.g. Leon-Rodriguez and Dickens, 2010; Westerhold et al., 2018), enhanced dissolution observed through the middle and late Eocene are consistent with lowered net carbon emissions. Effectively, the exogenic carbon cycle mass diminishes, less carbon comes into the ocean, less carbonate leaves via seafloor deposition, and the lysocline and CCD shoal. Following our study at Site 1209, clearly, there is room for additional work, because, circa 2020, it is difficult to arrive at good internally consistent explanations for how to link climate and carbonate accumulation in the deep-sea.

6. Conclusions

Our study at ODP Site 1209 in the north-central Pacific presents the first set of continuous records relevant to understanding changes in seafloor carbonate dissolution across the entire Eocene. We have generated records of bulk carbonate $\delta^{13}C$ and $\delta^{18}O$, carbonate content, and carbonate mass accumulation rates as in several studies. Here we also tie these to measurements that relate to seafloor carbonate dissolution and how various biogenic carbonate components respond to changes in ocean chemistry. The records are complex, certainly more so than we initially anticipated. Over both long-term and across short intervals, major changes in carbonate dissolution occurred. These can be summarized as:

- Transient increases in carbonate dissolution were associated with short-term early Eocene hyperthermals. Such increases were accompanied by negative carbon isotope excursions, rises in MS, and drops in carbonate content.
- During the middle-late Eocene, a number of prominent carbonate dissolution events happened at Shatsky Rise. These dissolution events seem stratigraphically correlated to high amplitude variations in the CCD previously recorded in the equatorial Pacific.
- The MECO exhibits intense carbonate dissolution, along with a prominent negative $\delta^{18}O$ excursion but a modest negative $\delta^{13}C$ excursion. Likely carbonate dissolution horizons in the equatorial Pacific shoaled during MECO.
- Considering long-term trends at Site 1209, seafloor carbonate dissolution appears relatively mild at Site 1209 through the middle of the EECO (~52 Ma). After this time, dissolution intensifies, and this change coincides with increase in $\delta^{13}C$ of both bulk carbonates and benthic foraminifers.
- Carbonate mass accumulation rates greatly increased between 52 and 48 Ma. Whether this reflects an anomalous increase in nannofossil productivity, the observation differs from expectations from the equatorial Pacific, where the CCD shoaled. This may indicate complex relations concerning deep-sea carbonate accumulation at sites lying below the lysocline.
- The intensity of carbonate dissolution significantly increases after 44 Ma. This contrasts with records from the Equatorial Pacific. Either tectonism and changes in seafloor depth have affected one or both regions, or a major shift in regional carbonate accumulation occurred.
- A prominent drop in seafloor carbonate dissolution occurred at the end of the Eocene epoch. This major change at or near the Eocene-Oligocene transition (EOT) has been documented many times.

Supplementary data to this article can be found online at https://doi.org/10.1016/j.sedgeo.2020.105705.

Declaration of competing interest

The authors declare that they have no known competing financial interests or personal relationships that could have appeared to influence the work reported in this paper.

Acknowledgement

We thank scientists and staff at the Gulf Coast Repository at College Station for sample collection, Dyke Andreasen and Colin Carney at the Stable Isotope Laboratory of University of California at Santa Cruz and Tao Sun at the Stable Isotope Laboratory of Rice University for performing isotope analyses on samples, and Benjamin Slotnick (BP) and Lizette Leon-Rodriguez (ExxonMobil) for mentoring on measurement of carbonate content of samples and calculation of dissolution indices, respectively. We thank Margot J. Cramwinckel and Valeria Luciani for very helpful comments and suggestions that improved the original manuscript submission. We thank Dr. Laurence Y. Yeung (Rice University) for helpful insights during manuscript preparation. This work was supported by an NSF grant awarded to Cin-Ty Lee, Gerald R. Dickens and other colleagues (NSF-FESD-OCE-1338842).

References

Agnini, C., Macrì, P., Backman, J., Brinkhuis, H., Fornaciari, E., Giusberti, L., Luciani, V., Rio, D., Sluijs, A., Speranza, F., 2009. An early Eocene carbon cycle perturbation at ~52.5 Ma in the Southern Alps: Chronology and biotic response. Paleoceanogr. Paleoclimatology., 24 https://doi.org/10.1029/2008PA001649.

Agnini, C., Spofforth, D., Dickens, G., Rio, D., Pälike, H., Backman, J., Muttoni, G., Dallanave, E., 2016. Stable isotope and calcareous nannofossil assemblage record of the late Paleocene and early Eocene (Cicogna section). Clim. Past 12. https://doi.org/10.5194/cp-12-883-2016.

Anagnostou, E., John, E.H., Edgar, K.M., Foster, G.L., Ridgwell, A., Inglis, G.N., Pancost, R.D., Lunt, D.J., Pearson, P.N., 2016. Changing atmospheric CO2 concentration was the primary driver of early Cenozoic climate. Nature 533, 380–384. https://doi.org/10.1038/nature17423.

Archer, D., 1996. A data-driven model of the global calcite lysocline. Glob. Biogeochem. Cycles 10, 511–526. https://doi.org/10.1029/96GB01521.

Armstrong McKay, D.I., Tyrrell, T., Wilson, P.A., 2016. Global carbon cycle perturbation across the Eocene-Oligocene climate transition. Paleoceanography 31, 311–329. https://doi.org/10.1002/2015PA002818.

Bassinot, F.C., Beaufort, L., Vincent, E., Labeyrie, L.D., Rostek, F., Müller, P.J., Quidelleur, X., Lancelot, Y., 1994. Coarse fraction fluctuations in pelagic carbonate sediments from the tropical Indian Ocean: a 1500-kyr record of carbonate dissolution. Paleoceanography 9, 579–600. https://doi.org/10.1029/94PA00860.

Bé, A.W., Morse, J.W., Harrison, S.M., 1975. Progressive dissolution and ultrastructural breakdown of planktonic foraminifera. Dissolution of Deep-sea Carbonates 13. Cushman Foundation for Foraminiferal Research.

Beerling, D.J., Royer, D.L., 2011. Convergent Cenozoic CO_2 history. Nat. Geosci. https://doi.org/10.1038/ngeo1186.

Berger, W.H., 1970. Biogenous deep-sea sediments: fractionation by deep-sea circulation. Geol. Soc. Am. Bull. 81 (5), 1385–1402.

Berger, W.H., 1973. Deep-sea carbonates: evidence for a coccolith lysocline. Deep-Sea Res. Oceanogr. Abstr. 20, 917–921. https://doi.org/10.1016/0011-7471(73)90110-1.

Berger, W.H., Adelseck, C.G., Mayer, L.A., 1976. Distribution of carbonate in surface sediments of the Pacific Ocean. J. Geophys. Res. 81, 2617–2627. https://doi.org/10.1029/jc081i015p02617.

Berger, W., Bonneau, M., Parker, F., 1982. Foraminifera on the deep-sea floor - lysocline and dissolution rate. Oceanol. Acta 5, 249–258.

Berggren, W.A., Kent, D.V., Swisher III, C.C., Aubry, M.-P., 1995. A revised Cenozoic geochronology and chronostratigraphy. In: Berggren, W.A., Kent, D.V., Aubry, M.-P., Hardenbol, J. (Eds.), Geochronology, Time Scales and Global Stratigraphic Correlation. Spec. Publ.—SEPM (Soc. Sediment. Geol.). 54, pp. 129–212.

Berner, R.A., 1991. A model for atmospheric CO_2 over phanerozoic time. Am. J. Sci. 291, 339–376.

Berner, R.A., Lasaga, A.C., Garrels, R.M., 1983. The carbonate-silicate geochemical cycle and its effect on atmospheric carbon dioxide over the past 100 million years. Am. J. Sci. 283, 641–683. https://doi.org/10.2475/ajs.283.7.641.

Bijl, P.K., Schouten, S., Sluijs, A., Reichart, G.J., Zachos, J.C., Brinkhuis, H., 2009. Early palaeogene temperature evolution of the southwest Pacific Ocean. Nature 461, 776–779. https://doi.org/10.1038/nature08399.

Bijl, P.K., Bendle, J.A., Bohaty, S.M., Schouten, S., Tauxe, L., Stickley, C.E., McKay, R.M., Röhl, U., Olney, M., Sluijs, A., 2013. Eocene cooling linked to early flow across the Tasmanian Gateway. Proc. Natl. Acad. Sci. 110 (24), 9645–9650.

Blanchet, C.L., Kasten, S., Vidal, L., Poulton, S.W., Ganeshram, R., Thouveny, N., 2012. Influence of diagenesis on the stable isotopic composition of biogenic carbonates from the Gulf of Tehuantepec oxygen minimum zone. Geochem. Geophys. Geosyst. 13. https://doi.org/10.1029/2011GC003800.

Bohaty, S.M., Zachos, J.C., 2003. Significant Southern Ocean warming event in the late middle Eocene. Geology 31, 1017. https://doi.org/10.1130/G19800.1.

Bohaty, S.M., Zachos, J.C., Florindo, F., Delaney, M.L., 2009. Coupled greenhouse warming and deep-sea acidification in the middle Eocene. Paleoceanography 24 (2).

Boscolo Galazzo, F., Thomas, E., Pagani, M., Warren, C., Luciani, V., Giusberti, L., 2014. The middle Eocene climatic optimum (MECO): a multiproxy record of paleoceanographic changes in the Southeast Atlantic (ODP Site 1263, Walvis Ridge). Paleoceanography 29, 1143–1161. https://doi.org/10.1002/2014PA002670.

Boudagher-Fadel, M.K., 2018. Biostratigraphic and Geological Significance of Planktonic Foraminifera, Biostratigraphic and Geological Significance of Planktonic Foraminifera. UCL Press https://doi.org/10.2307/j.ctt1g69xwk.

Boudreau, B.P., Middelburg, J.J., Meysman, F.J.R., 2010. Carbonate compensation dynamics. Geophys. Res. Lett. 37. https://doi.org/10.1029/2009GL041847.

Bralower, T.J., 2005. Paleocene–early Oligocene calcareous nannofossil biostratigraphy, ODP Leg 198 Sites 1209, 1210, and 1211 (Shatsky Rise, Pacific Ocean). Proceedings of the Ocean Drilling Program, Scientific Results. 198.

Bralower, T.J., Premoli Silva, I., Malone, M.J., et al., 2002. Proceedings of the Ocean Drilling Program. Leg, Initial Reports, p. 198. http://www-odp.tamu.edu/publications/198_IR/198ir.htm.

Broecker, W.S., 2008. A need to improve reconstructions of the fluctuations in the calcite compensation depth over the course of the Cenozoic. Paleoceanography 23. https://doi.org/10.1029/2007PA001456.

Broecker, W.S., Peng, T.-H., 1982. Tracers in the Sea.

Carter, A., Riley, T.R., Hillenbrand, C.D., Rittner, M., 2017. Widespread Antarctic glaciation during the Late Eocene. Earth Planet. Sci. Lett. 458, 49–57. https://doi.org/10.1016/j.epsl.2016.10.045.

Chiu, T.-C., Broecker, W.S., 2008. Toward better paleocarbonate ion reconstructions: New insights regarding the $CaCO_3$ size index. Paleoceanography 23. https://doi.org/10.1029/2008PA001599.

Colosimo, A.B., Bralower, T.J., Zachos, J.C., 2006. Evidence for lysocline shoaling at the Paleocene/Eocene Thermal Maximum on Shatsky Rise, Northwest Pacific. Proceedings of the Ocean Drilling Program, Scientific Results, p. 198.

Coxall, H.K., Wilson, P.A., Pälike, H., Lear, C.H., Backman, J., 2005. Rapid stepwise onset of Antarctic glaciation and deeper calcite compensation in the Pacific Ocean. Nature 433, 53–57. https://doi.org/10.1038/nature03135.

Cramer, B.S., Toggweiler, J.R., Wright, J.D., Katz, M.E., Miller, K.G., 2009. Ocean overturning since the late cretaceous: Inferences from a new benthic foraminiferal isotope compilation. Paleoceanography 24. https://doi.org/10.1029/2008PA001683.

Cramwinckel, M.J., Huber, M., Kocken, I.J., Agnini, C., Bijl, P.K., Bohaty, S.M., Frieling, J., Goldner, A., Hilgen, F.J., Kip, E.L., Peterse, F., Van Der Ploeg, R., Röhl, U., Schouten, S., Sluijs, A., 2018. Synchronous tropical and polar temperature evolution in the Eocene letter. Nature 559, 382–386. https://doi.org/10.1038/s41586-018-0272-2.

Cramwinckel, M.J., Woelders, L., Huurdeman, E.P., Peterse, F., Gallagher, S.J., Pross, J., Burgess, C., Reichart, G.-J., Sluijs, A., Bijl, P.K., 2019. Surface-circulation change in the Southern Ocean across the Middle Eocene Climatic Optimum: inferences from dinoflagellate cysts and biomarker paleothermometry. Clim. Past Discuss., 1–34 https://doi.org/10.5194/cp-2019-35.

Cros, L., Fortuño, J.M., 2002. Atlas of Northwestern Mediterranean Coccolithophores. Sci. Mar. 66, 1–182. https://doi.org/10.3989/scimar.2002.66s11.

Crouch, E.M., Shepherd, C.L., Morgans, H.E.G., Naafs, B.D.A., Dallanave, E., Phillips, A., Hollis, C.J., Pancost, R.D., 2020. Climatic and environmental changes across the early Eocene climatic optimum at mid-Waipara River, Canterbury Basin, New Zealand. Earth Sci. Rev. https://doi.org/10.1016/j.earscirev.2019.102961.

Dickens, G.R., 1995. Dissociation of oceanic methane hydrate as a cause of the carbon isotope excursion at the end of Paleocene. Paleoceanography 10, 965–971.

Dickens, G.R., 1999. The blast in the past. Nature 401, 752–755.

Dickens, G.R., 2003. Rethinking the global carbon cycle with a large, dynamic and microbially mediated gas hydrate capacitor. Earth Planet. Sci. Lett. 213, 169–183. https://doi.org/10.1016/S0012-821X(03)00325-X.

Dickens, G.R., Backman, J., 2013. Core alignment and composite depth scale for the lower Paleogene through uppermost cretaceous interval at deep-sea drilling project site 577. Newsl. Stratigr. 46, 47–68. https://doi.org/10.1127/0078-0421/2013/0027.

Dickens, G.R., Castillo, M.M., Walker, J.C.G., 1997. A blast of gas in the latest Paleocene: Simulating first-order effects of massive dissociation of oceanic methane hydrate. Geology 25, 259–262. https://doi.org/10.1130/0091-7613(1997)025<0259:abogit>2.3.co;2.

D'Onofrio, R., Luciani, V., Dickens, G.R., Wade, B.S., Kirtland Turner, S., 2020. Demise of the planktic foraminifer genus *Morozovella* during the Early Eocene climatic optimum: new records from ODP Site 1258 (Demerara rise, Western Equatorial Atlantic) and site 1263 (Walvis Ridge, South Atlantic). Geosciences 10, 88. https://doi.org/10.3390/geosciences10030088.

Dunn, D.A., 1980. Revised techniques for quantitative calcium carbonate analysis using the' Karbonat-Bombe', and comparisons to other quantitative carbonate analysis methods. J. Sediment. Petrol. 50, 631–637. https://doi.org/10.2110/jsr.50.631.

Dutton, A., Lohmann, K.C., Leckie, R.M., 2005. Insights From the Paleogene Tropical Pacific: Foraminiferal Stable Isotope and Elemental Results From Site 1209, Shatsky Rise. https://doi.org/10.1029/2004PA001098.

Edgar, K.M., Anagnostou, E., Pearson, P.N., Foster, G.L., 2015. Assessing the impact of diagenesis on δ11B, δ13C, δ18O, Sr/Ca and B/Ca values in fossil planktic foraminiferal calcite. Geochim. Cosmochim. Acta 166, 189–209. https://doi.org/10.1016/j.gca.2015.06.018.

Ellwood, B.B., Crick, R.E., El Hassani, A., Benoist, S.L., Young, R.H., 2000. Magnetosusceptibility event and cyclostratigraphy method applied to marine rocks: detrital input versus carbonate productivity. Geology 28, 1135–1138. https://doi.org/10.1130/0091-7613(2000)28<1135:meacma>2.0.co;2.

Frenz, M., Baumann, K.-H., Boeckel, B., Hoppner, R., Henrich, R., 2005. Quantification of foraminifer and coccolith carbonate in South Atlantic surface sediments by means of carbonate grain-size distributions. J. Sediment. Res. 75, 464–475. https://doi.org/10.2110/jsr.2005.036.

Greene, S.E., Ridgwell, A., Kirtland Turner, S., Schmidt, D.N., Pälike, H., Thomas, E., Greene, L.K., Hoogakker, B.A.A., 2019. Early cenozoic decoupling of climate and carbonate compensation depth trends. Paleoceanogr. Paleoclimatology 34, 930–945. https://doi.org/10.1029/2019PA003601.

Hancock, H.J., Dickens, G.R., 2005. Carbonate dissolution episodes in Paleocene and Eocene sediment, Shatsky Rise, West-Central Pacific. Proceedings of the Ocean Drilling Program, Scientific Results, p. 198.

Hancock, H.J.L., Dickens, G.R., Thomas, E., Blake, K.L., 2007. Reappraisal of early Paleogene CCD curves: foraminiferal assemblages and stable carbon isotopes across the carbonate facies of Perth Abyssal Plain. Int. J. Earth Sci. 96, 925–946. https://doi.org/10.1007/s00531-006-0144-0.

Henehan, M.J., Edgar, K.M., Foster, G.L., Penman, D.E., Hull, P.M., Greenop, R., Anagnostou, E., Pearson, P.N., 2020. Revisiting the Middle Eocene Climatic Optimum 'Carbon Cycle Conundrum' with new estimates of atmospheric pCO_2 from boron isotopes. Paleoceanogr. Paleoclimatology https://doi.org/10.1029/2019PA003713.

Hollis, C.J., Handley, L., Crouch, E.M., Morgans, H.E.G., Baker, J.A., Creech, J., Collins, K.S., Gibbs, S.J., Huber, M., Schouten, S., Zachos, J.C., Pancost, R.D., 2009. Tropical sea temperatures in the high-latitude South Pacific during the Eocene. Geology 37, 99–102. https://doi.org/10.1130/G25200A.1.

Hönisch, B., Ridgwell, A., Schmidt, D.N., Thomas, E., Gibbs, S.J., Sluijs, A., Zeebe, R., Kump, L., Martindale, R.C., Greene, S.E., Kiessling, W., Ries, J., Zachos, J.C., Royer, D.L., Barker, S., Marchitto, T.M., Moyer, R., Pelejero, C., Ziveri, P., Foster, G.L., Williams, B., 2012. The geological record of ocean acidification. Science 335, 1058–1063. https://doi.org/10.1126/science.1208277.

Ito, G., Clift, P.D., 1998. Subsidence and growth of Pacific Cretaceous plateaus. Earth Planet. Sci. Lett. 161 (1–4), 85–100.

Keith, M.L., Weber, J.N., 1964. Carbon and oxygen isotopic composition of selected limestones and fossils. Geochim. Cosmochim. Acta 28, 1787–1816. https://doi.org/10.1016/0016-7037(64)90022-5.

Kelly, D.C., Nielsen, T.M.J., McCarren, H.K., Zachos, J.C., Röhl, U., 2010. Spatiotemporal patterns of carbonate sedimentation in the South Atlantic: implications for carbon cycling during the Paleocene-Eocene thermal maximum. Palaeogeogr. Palaeoclimatol. Palaeoecol. 293, 30–40. https://doi.org/10.1016/j.palaeo.2010.04.027.

Kirtland Turner, S., 2018. Constraints on the onset duration of the Paleocene-Eocene thermal maximum. Philos. Trans. R. Soc. A Math. Phys. Eng. Sci. https://doi.org/10.1098/rsta.2017.0082.

Kirtland Turner, S., Ridgwell, A., 2016. Development of a novel empirical framework for interpreting geological carbon isotope excursions, with implications for the rate of carbon injection across the PETM. Earth Planet. Sci. Lett. 435, 1–13. https://doi.org/10.1016/j.epsl.2015.11.027.

Kirtland Turner, S., Sexton, P.F., Charles, C.D., Norris, R.D., 2014. Persistence of carbon release events through the peak of early Eocene global warmth. Nat. Geosci. 7, 748–751. https://doi.org/10.1038/NGEO2240.

Komar, N., Zeebe, R.E., Dickens, G.R., 2013. Understanding long-term carbon cycle trends: the late Paleocene through the early Eocene. Paleoceanography 28, 1–13. https://doi.org/10.1002/palo.20060.

Kump, L.R., 1991. Interpreting carbon-isotope excursions: strangelove oceans. Geology 19, 299–302. https://doi.org/10.1130/0091-7613(1991)019<0299:icieso>2.3.co;2.

Kump, L.R., Arthur, M.A., 1999. Interpreting carbon-isotope excursions: carbonates and organic matter. Chem. Geol. 161, 181–198. https://doi.org/10.1016/S0009-2541(99)00086-8.

Kump, L.R., Brantley, S.L., Arthur, M.A., 2000. Chemical weathering, Atmospheric CO_2, and climate. Annu. Rev. Earth Planet. Sci. 28, 611–667. https://doi.org/10.1146/annurev.earth.28.1.611.

Kump, L., Bralower, T., Ridgwell, A., 2009. Ocean acidification in deep time. Oceanography 22, 94–107. https://doi.org/10.5670/oceanog.2009.100.

Lauretano, V., Littler, K., Polling, M., Zachos, J.C., Lourens, L.J., 2015. Frequency, magnitude and character of hyperthermal events at the onset of the Early Eocene climatic optimum. Clim. Past 11, 1313–1324. https://doi.org/10.5194/cp-11-1313-2015.

Lauretano, V., Hilgen, F.J., Zachos, J.C., Lourens, L.J., 2016. Astronomically tuned age model for the early Eocene carbon isotope events: a new high-resolution δ13Cbenthic record of ODP Site 1263 between ~49 and ~54 Ma. Newsl. Stratigr. 49, 383–400. https://doi.org/10.1127/nos/2016/0077.

Le, J., Shackleton, N.J., 1992. Carbonate dissolution fluctuations in the western equatorial pacific during the Late Quaternary. Paleoceanography 7, 21–42. https://doi.org/10.1029/91PA02854.

Leon-Rodriguez, L., Dickens, G.R., 2010. Constraints on ocean acidification associated with rapid and massive carbon injections: the early Paleogene record at ocean drilling program site 1215, equatorial Pacific Ocean. Palaeogeogr. Palaeoclimatol. Palaeoecol. 298, 409–420. https://doi.org/10.1016/j.palaeo.2010.10.029.

Littler, K., Röhl, U., Westerhold, T., Zachos, J.C., 2014. A high-resolution benthic stable-isotope record for the South Atlantic: implications for orbital-scale changes in Late Paleocene-Early Eocene climate and carbon cycling. Earth Planet. Sci. Lett. 401, 18–30. https://doi.org/10.1016/j.epsl.2014.05.054.

Lohmann, G.P., 1995. A model for variation in the chemistry of planktonic foraminifera due to secondary calcification and selective dissolution. Paleoceanography 10, 445–457. https://doi.org/10.1029/95PA00059.

Lourens, L.J., Sluijs, A., Kroon, D., Zachos, J.C., Thomas, E., Röhl, U., Bowles, J., Raffi, I., 2005. Astronomical pacing of late Palaeocene to early Eocene global warming events. Nature 435, 1083–1087. https://doi.org/10.1038/nature03814.

Lu, G., Keller, G., 1993. The Paleocene-Eocene transition in the Antarctic Indian Ocean: inference from planktic foraminifera. Mar. Micropaleontol. 21, 101–142. https://doi.org/10.1016/0377-8398(93)90012-M.

Luciani, V., Dickens, G.R., Backman, J., Fornaciari, E., Giusberti, L., Agnini .D., C., Onofrio, R., 2016. Major perturbations in the global carbon cycle and photosymbiont-bearing planktic foraminifera during the early Eocene. Clim. Past 12, 981–1007. https://doi.org/10.5194/cp-12-981-2016.

Lyle, M.W., Olivarez Lyle, A., Backman, J., Tripati, A., 2005. Biogenic sedimentation in the Eocene equatorial Pacific—the stuttering greenhouse and Eocene carbonate compensation depth. Proceedings of the Ocean Drilling Program, Scientific Results, p. 199.

Malmgren, B.A., 1987. Differential dissolution of Upper Cretaceous planktonic foraminifera from a temperate region of the South Atlantic Ocean. Mar. Micropaleontol. 11, 251–271. https://doi.org/10.1016/0377-8398(87)90001-6.

Merico, A., Tyrrell, T., Wilson, P.A., 2008. LETTERS Eocene/Oligocene Ocean deacidification Linked to Antarctic Glaciation by Sea-level Fall. , p. 452. https://doi.org/10.1038/nature06853.

Millero, F.J., 1995. Thermodynamics of the carbon dioxide system in the oceans. Geochim. Cosmochim. Acta 59, 661–677. https://doi.org/10.1016/0016-7037(94)00354-O.

Mucci, A., 1983. The solubility of calcite and aragonite in seawater at various salinities, temperatures, and one atmosphere total pressure. Am. J. Sci. 283, 780–799.

Müller, G., Gastner, M., 1971. The 'Karbonat-Bombe', a simple device for the determination of carbonate content in sediment, soils, and other materials. Neues Jahrb. Mineral. Monatshefte 10, 466–469.

Nguyen, T.M.P., Petrizzo, M.R., Speijer, R.P., 2009. Experimental dissolution of a fossil foraminiferal assemblage (Paleocene-Eocene thermal maximum, Dababiya, Egypt): implications for paleoenvironmental reconstructions. Mar. Micropaleontol. 73, 241–258. https://doi.org/10.1016/j.marmicro.2009.10.005.

Nicolo, M.J., Dickens, G.R., Hollis, C.J., Zachos, J.C., 2007. Multiple early Eocene hyperthermals: their sedimentary expression on the New Zealand continental margin and in the deep-sea. Geology 35, 699. https://doi.org/10.1130/G23648A.1.

Norris, R.D., Wilson, P.A., Blum, P., the Expedition 342 Scientists, 2014. Proc. IODP, 342: College Station, TX (Integrated Ocean Drilling Program). https://doi.org/10.2204/iodp.proc.342.102.2014.

O'Connor, J.M., Hoernle, K., Dietmar Müller, R., Morgan, J.P., Butterworth, N.P., Hauff, F., Sandwell, D.T., Jokat, W., Wijbrans, J.R., Stoffers, P., 2015. Deformation-related volcanism in the Pacific Ocean linked to the Hawaiian-Emperor bend. Nat. Geosci. 8, 393–397. https://doi.org/10.1038/ngeo2416.

Okada, H., Bukry, D., 1980. Supplementary modification and introduction of code numbers to the low-latitude coccolith biostratigraphic zonation (Bukry, 1973; 1975). Mar. Micropaleontol. 5, 321–325.

Pagani, M., Zachos, J.C., Freeman, K.H., Tipple, B., Bohaty, S., 2005. Marked decline in atmospheric carbon dioxide concentrations during the paleogene. Science 309 (80-.).

Pagani, M., Huber, M., Liu, Z., Bohaty, S.M., Henderiks, J., Sijp, W., Krishnan, S., DeConto, R.M., 2011. The role of carbon dioxide during the onset of antarctic glaciation. Science 334, 1261–1264. https://doi.org/10.1126/science.1203909 (80-.).

Pälike, H., Lyle, M.W., Nishi, H., Raffi, I., Ridgwell, A., Gamage, K., Klaus, A., Acton, G., Anderson, L., Backman, J., Baldauf, J., Beltran, C., Bohaty, S.M., Bown, P., Busch, W., Channell, J.E.T., Chun, C.O.J., Delaney, M., Dewangan, P., Dunkley Jones, T., Edgar, K. M., Evans, H., Fitch, P., Foster, G.L., Gussone, N., Hasegawa, H., Hathorne, E.C., Hayashi, H., Herrle, J.O., Holbourn, A., Hovan, S., Hyeong, K., Iijima, K., Ito, T., Kamikuri, S., Kimoto, K., Kuroda, J., Leon-Rodriguez, L., Malinverno, A., Moore Jr., T. C., Murphy, B.H., Murphy, D.P., Nakamura, H., Ogane, K., Ohneiser, C., Richter, C., Robinson, R., Rohling, E.J., Romero, O., Sawada, K., Scher, H., Schneider, L., Sluijs, A., Takata, H., Tian, J., Tsujimoto, A., Wade, B.S., Westerhold, T., Wilkens, R., Williams, T., Wilson, P.A., Yamamoto, Y., Yamamoto, S., Yamazaki, T., Zeebe, R.E., 2012. A Cenozoic record of the equatorial Pacific carbonate compensation depth. Nature 488, 609.

Pearson, P.N., Ditchfield, P.W., Singano, J., Harcourt-Brown, K.G., Nicholas, C.J., Olsson, R.K., Shackleton, N.J., Hall, M.A., 2001. Warm tropical sea surface temperatures in the Late Cretaceous and Eocene epochs. Nature. https://doi.org/10.1038/35097000.

Penman, D.E., Hönisch, B., Zeebe, R.E., Thomas, E., Zachos, J.C., 2014. Rapid and sustained surface ocean acidification during the Paleocene-Eocene thermal maximum. Paleoceanography 29, 357–369. https://doi.org/10.1002/2014PA002621.

Penman, D.E., Turner, S.K., Sexton, P.F., Norris, R.D., Dickson, A.J., Boulila, S., Ridgwell, A., Zeebe, R.E., Zachos, J.C., Cameron, A., Westerhold, T., Röhl, U., 2016. An abyssal carbonate compensation depth overshoot in the aftermath of the Palaeocene–Eocene thermal maximum. Nat. Geosci. 9, 575.

Petrizzo, M.R., Leoni, G., Speijer, R.P., De Bernardi, B., Felletti, F., 2008. Dissolution susceptibility of some Paleogene planktonic foraminifera from ODP site 1209 (Shatsky Rise, Pacific Ocean). J. Foraminifer. Res. 38 (4), 357–371.

Rea, D.K., Lyle, M.W., 2005. Paleogene calcite compensation depth in the eastern subtropical Pacific: answers and questions. Paleoceanography 20. https://doi.org/10.1029/2004PA001064.

Reghellin, D., Coxall, H.K., Dickens, G.R., Backman, J., 2015. Carbon and oxygen isotopes of bulk carbonate in sediment deposited beneath the eastern equatorial Pacific over the last 8 million years. Paleoceanography 30, 1261–1286. https://doi.org/10.1002/2015PA002825.

Reghellin, D., Dickens, G.R., Coxall, H.K., Backman, J., 2020. Understanding bulk sediment stable isotope records in the Eastern Equatorial pacific, from seven million years ago to present day. Paleoceanogr. Paleoclimatology 35. https://doi.org/10.1029/2019PA003586.

Ridgwell, A., Zeebe, R.E., 2005. The role of the global carbonate cycle in the regulation and evolution of the Earth system. Earth Planet. Sci. Lett. 234, 299–315. https://doi.org/10.1016/j.epsl.2005.03.006.

Romanek, C.S., Grossman, E.L., Morse, J.W., 1992. Carbon isotopic fractionation in synthetic aragonite and calcite: effects of temperature and precipitation rate. Geochim. Cosmochim. Acta 56, 419–430. https://doi.org/10.1016/0016-7037(92)90142-6.

Royer, Dana L., Berner, Robert A., Montañez, Isabel P., Tabor, Neil J., Beerling, D.J., 2004. CO2 as a primary driver of Phanerozoic climate. GSA Today 14. https://doi.org/10.1130/1052-5173(2004)014<4:CAAPDO>2.0.CO;2.

Sager, W.W., Kim, J., Klaus, A., Nakanishi, M., Khankishieva, L.M., 1999. Bathymetry of Shatsky Rise, northwest Pacific Ocean: implications for ocean plateau development at a triple junction. J. Geophys. Res. Solid Earth 104, 7557–7576. https://doi.org/10.1029/1998jb900009.

Schrag, D.P., 1999. Effects of diagenesis on the isotopic record of late paleogene tropical sea surface temperatures. Chem. Geol. 161, 215–224. https://doi.org/10.1016/S0009-2541(99)00088-1.

Schrag, D.P., Depaolo, D.J., Richter, F.M., 1995. Reconstructing past sea surface temperatures: Correcting for diagenesis of bulk marine carbonate. Geochim. Cosmochim. Acta 59 (11), 2265–2278.

Sexton, P.F., Wilson, P.A., Pearson, P.N., 2006. Microstructural and geochemical perspectives on planktic foraminiferal preservation: "Glassy" versus "Frosty.". Geochem. Geophys. Geosyst. 7. https://doi.org/10.1029/2006GC001291 n/a-n/a.

Shackleton, N.J., Hall, M.A., 1984. Oxygen and carbon isotope stratigraphy of Deep-sea Drilling Project Hole 552A: plio-Pleostocene glacial history. Initial Rep. Deep Sea Drill. Proj. 81, 599–609.

Shackleton, N.J., Hall, M.A., Bleil, U., Heath, R.G., Buckle, L.H., et al., 1985. Carbon isotope startigraphy Site 577. Initial Rep. Deep Sea Drill. Proj. 86, 503–512.

Slotnick, B.S., Lauretano, V., Backman, J., Dickens, G.R., Sluijs, A., Lourens, L., 2015. Early Paleogene variations in the calcite compensation depth: new constraints using old borehole sediments from across Ninetyeast Ridge, central Indian Ocean. Clim. Past 11, 473–493. https://doi.org/10.5194/cp-11-473-2015.

Sluijs, A., Schouten, S., Donders, T.H., Schoon, P.L., Röhl, U., Reichart, G.J., Sangiorgi, F., Kim, J.H., Sinninghe Damsté, J.S., Brinkhuis, H., 2009. Warm and wet conditions in the Arctic region during Eocene thermal Maximum 2. Nat. Geosci. 2, 777–780. https://doi.org/10.1038/ngeo668.

Sluijs, A., Zeebe, R.E., Bijl, P.K., Bohaty, S.M., 2013. A middle Eocene carbon cycle conundrum. Nat. Geosci. 6, 429.

Stap, L., Sluijs, A., Thomas, E., Lourens, L., 2009. Patterns and magnitude of deep-sea carbonate dissolution during Eocene thermal Maximum 2 and H2, Walvis Ridge, southeastern Atlantic Ocean. Paleoceanography 24. https://doi.org/10.1029/2008PA001655.

Stap, L., Lourens, L.J., Thomas, E., Sluijs, A., Bohaty, S., Zachos, J.C., 2010. High-resolution deep-sea carbon and oxygen isotope records of Eocene thermal Maximum 2 and H2. Geology 38, 607–610. https://doi.org/10.1130/G30777.1.

Sulpis, O., Boudreau, B.P., Mucci, A., Jenkins, C., Trossman, D.S., Arbic, B.K., Key, R.M., 2018. Current CaCO3 dissolution at the seafloor caused by anthropogenic CO_2. Proc. Natl. Acad. Sci. U. S. A. 115, 11700–11705. https://doi.org/10.1073/pnas.1804250115.

Sutherland, R., Dickens, G.R., Blum, P., Agnini, C., Alegret, L., Asatryan, G., Bhattacharya, J., Bordenave, A., Chang, L., Collot, J., Cramwinckel, M.J., Dallanave, E., Drake, M.K., Etienne, S.J.G., Giorgioni, M., Gurnis, M., Harper, D.T., Huang, H.-H.M., Keller, A.L., Lam, A.R., Li, H., Matsui, H., Morgans, H.E.G., Newsam, C., Park, Y.-H., Pascher, K.M., Pekar, S.F., Penman, D.E., Saito, S., Stratford, W.R., Westerhold, T., Zhou, X., 2020. Continental-scale geographic change across Zealandia during Paleogene subduction initiation. Geol. Soc. Am. Geol. 1. https://doi.org/10.1130/G47008.1.

Thomas, E., Shackleton, N.J., 1996. The Paleocene-Eocene benthic foraminiferal extinction and stable isotope anomalies. Geol. Soc. Spec. Publ. 101, 401–441. https://doi.org/10.1144/GSL.SP.1996.101.01.20.

Thunell, R.C., 1976. Optimum indices of calcium carbonate dissolution, in deep-sea sediments. Geology 4, 525–528. https://doi.org/10.1130/0091-7613(1976)4<525:oioccd>2.0.co;2.

van Andel, T.H., 1975. Mesozoic/cenozoic calcite compensation depth and the global distribution of calcareous sediments. Earth Planet. Sci. Lett. 26, 187–194. https://doi.org/10.1016/0012-821X(75)90086-2.

van Andel, T.H., 1983. Estimation of sedimentation and accumulation rates. In: Health, G. G. (Ed.), Sedimentology, Physical Properties and Geochemistry in the Initial Reports of the Deep-Sea Drilling Project: An Overview. National Oceanic Atmphospheric Administration. Environemnta; and Information Data Service, Boulder, CO, pp. 93–101.

van der Ploeg, R., Selby, D., Cramwinckel, M.J., Li, Y., Bohaty, S.M., Middelburg, J.J., Sluijs, A., 2018. Middle Eocene greenhouse warming facilitated by diminished weathering feedback. Nat. Commun. 9, 1–10. https://doi.org/10.1038/s41467-018-05104-9.

Westerhold, T., Röhl, U., 2006. Revised composite depth records for Shatsky Rise Sites 1209, 1210, and 1211. Proceedings of the Ocean Drilling Program, Scientific Results, 198.

Westerhold, T., Röhl, U., Mccarren, H.K., Zachos, J.C., 2009. Latest on the absolute age of the Paleocene-Eocene thermal Maximum (PETM): new insights from exact stratigraphic position of key ash layers +19 and −17. Earth Planet. Sci. Lett. 287, 412–419. https://doi.org/10.1016/j.epsl.2009.08.027.

Westerhold, T., Röhl, U., Frederichs, T., Agnini, C., Raffi, I., Zachos, J.C., Wilkens, R.H., 2017. Astronomical calibration of the Ypresian timescale: implications for seafloor spreading rates and the chaotic behavior of the solar system? Clim. Past 13, 1129–1152. https://doi.org/10.5194/cp-13-1129-2017.

Westerhold, T., Röhl, U., Donner, B., Zachos, J.C., 2018. Global extent of early Eocene hyperthermal events: a New Pacific Benthic Foraminiferal Isotope record from Shatsky Rise (ODP Site 1209). Paleoceanogr. Paleoclimatology 33, 626–642. https://doi.org/10.1029/2017PA003306.

Zachos, J., Pagani, H., Sloan, L., Thomas, E., Billups, K., 2001. Trends, rhythms, and aberrations in global climate 65 Ma to present. Science https://doi.org/10.1126/science.1059412 (80-.).

Zachos, J.C., Kroon, D., Blum, P., et al., 2004. Proceedings of the Ocean Drilling Program, Initial Reports, Leg. , p. 208. https://doi.org/10.2973/odp.proc.ir.208.2004.

Zachos, J.C., Röhl, U., Schellenberg, S.A., Sluijs, A., Hodell, D.A., Kelly, D.C., Thomas, E., Nicolo, M., Raffi, I., Lourens, L.J., McCarren, H., Kroon, D., 2005. Paleoclimate: rapid acidification of the ocean during the paleocene-eocene thermal maximum. Science 308, 1611–1615. https://doi.org/10.1126/science.1109004.

Zachos, J.C., Bohaty, S.M., John, C.M., McCarren, H., Kelly, D.C., Nielsen, T., 2007. The Palaeocene-Eocene carbon isotope excursion: constraints from individual shell planktonic foraminifer records. Philos. Trans. R. Soc. A Math. Phys. Eng. Sci. 365, 1829–1842. https://doi.org/10.1098/rsta.2007.2045.

Zachos, J.C., Dickens, G.R., Zeebe, R.E., 2008. An early Cenozoic perspective on greenhouse warming and carbon-cycle dynamics. Nature. https://doi.org/10.1038/nature06588.

Zachos, J.C., McCarren, H., Murphy, B., Röhl, U., Westerhold, T., 2010. Tempo and scale of late Paleocene and early Eocene carbon isotope cycles: Implications for the origin of hyperthermals. Earth Planet. Sci. Lett. 299, 242–249. https://doi.org/10.1016/j.epsl.2010.09.004.

Zeebe, R.E., Westbroek, P., 2003. A simple model for the $CaCO_3$ saturation state of the ocean: the “Strangelove,” the “Neritan,” and the “Cretan” Ocean. Geochem. Geophys. Geosyst. 4. https://doi.org/10.1029/2003GC000538.

Zeebe, R.E., Zachos, J.C., Dickens, G.R., 2009. Carbon dioxide forcing alone insufficient to explain Palaeocene-Eocene thermal maximum warming. Nat. Geosci. 2, 576–580. https://doi.org/10.1038/ngeo578.